

# A Space-Time Multigrid Method for Space-Time Finite Element Discretizations of Parabolic and Hyperbolic PDEs

Nils Margenberg<sup>\*</sup>      Peter Munch<sup>†</sup>

We present a space-time multigrid method based on tensor-product space-time finite element discretizations. The method is facilitated by the matrix-free capabilities of the deal.II library. It addresses both high-order continuous and discontinuous variational time discretizations with spatial finite element discretizations. The effectiveness of multigrid methods in large-scale stationary problems is well established. However, their application in the space-time context poses significant challenges, mainly due to the construction of suitable smoothers. To address these challenges, we develop a space-time cell-wise additive Schwarz smoother and demonstrate its effectiveness on the heat and acoustic wave equations.

The matrix-free framework of the deal.II library supports various multigrid strategies, including  $h$ -,  $p$ -, and  $hp$ -refinement across spatial and temporal dimensions. Extensive empirical evidence, provided through scaling and convergence tests on high-performance computing platforms, demonstrate high performance on perturbed meshes and problems with heterogeneous and discontinuous coefficients. Throughputs of over a billion degrees of freedom per second are achieved on problems with more than a trillion global degrees of freedom. The results prove that the space-time multigrid method can effectively solve complex problems in high-fidelity simulations and show great potential for use in coupled problems.

MSC2020: 65M60, 65M55, 65F10, 65Y05

Keywords: *space-time finite elements, space-time multigrid, matrix-free, high-order, high-performance computing, tensor-product*

## 1 Introduction

In the recent years, parallel computing has become increasingly important for improving the efficiency and reducing computation times of numerical solutions for partial differential equations (PDEs). One significant area of research has been the development of space-time finite element methods and parallel time integration techniques, which aim to take advantage of spatial and temporal parallelism.

We present a space-time multigrid (STMG) method utilizing tensor-product space-time finite elements within the deal.II library framework [6, 41]. This approach combines high-order variational time discretizations with spatial finite elements to extend efficient multigrid methods to space-time problems. Employing a space-time cell-wise additive Schwarz method (ASM) as the smoother, we demonstrate high performance for heat and acoustic wave equations on perturbed meshes and problems with heterogeneous coefficients. Our scalable implementation is validated through tests on high-performance computing platforms and available on GitHub <https://github.com/nlsmrg/dealii-stfem>.

---

<sup>\*</sup>Helmut Schmidt University, Faculty of Mechanical and Civil Engineering, Holstenhofweg 85, 22043 Hamburg, Germany, [margenbn@hsu-hh.de](mailto:margenbn@hsu-hh.de) (Corresponding Author)

<sup>†</sup>Uppsala University, Department of Information Technology, Box 337, Uppsala, 75105, Sweden, [peter.munch@it.uu.se](mailto:peter.munch@it.uu.se)

Further investigations on space-time finite element methods have been done in [18, 19, 42], where numerical results with an adaptive algorithm are presented. The advantages of the variational time discretization are the natural integration with the variational space discretization and the natural capture of coupled problems and nonlinearities. Space-time finite elements are particularly advantageous for the use of concepts such as duality and goal-oriented adaptivity in space and time [59, 9, 57]. The concepts of variational space-time discretization also provide a unified approach to stability and error analysis as shown in [46].

While this paper deals with tensor-product space-time finite element methods, there are other approaches to space-time finite elements, particularly for perturbed space-time meshes. These are discussed in detail in [45] and [61, 18, 44, 52, 21, 45, 44]. These papers highlight the flexibility and effectiveness of the method in dealing with complex, time-dependent problems. Other notable examples include the work of [8, 32], as well as more recent developments such as those presented in [56, 63]. These works and their references serve as a good basis for a comprehensive survey of recent developments in space-time discretization techniques.

While time parallelism arises naturally in the context of space-time finite element methods, parallel time integration is a much broader topic. Most methods are based on time-domain decomposition techniques and rely on predictor-corrector algorithms, multilevel, multigrid, or multi-shooting methods. See [28, 53] for surveys on time parallelism. In particular, we mention work related to multigrid methods [24, 20, 16]. In addition to time-domain decomposition approaches, there is also stage parallelism, i. e. parallelism within a single time step, see for example [14, 55, 51]. The scalability of these methods is constrained by the number of stages, which may result in less parallelization potential than domain decomposition approaches, for example. Despite this limitation, these methods have been shown to be effective in the scaling limit [51], which is the main motivation for time parallelism in the first place.

There are two approaches to extending classical multigrid methods to the time dimension: multigrid-in-time and space-time multigrid. In recent years, significant work has been done on the multigrid-reduction-in-time (MGRIT) algorithm [24, 35, 29, 65], which is based on multigrid in time. An advantage of MGRIT is its easy integration into existing codes. It only requires a routine to integrate from one time to the next with an adjustable time step. STMG methods, on the other hand, have the full advantage of computing multiple time steps at once [39, 27, 23, 10, 17, 38]. Note that sequential time stepping is already optimal in terms of the complexity, but doesn't provide any parallel scalability. Therefore, paying with computational complexity to get better scalability is a viable option. In STMG methods, time is simply another dimension in the grid. Therefore, given a suitable smoother, they are of optimal complexity. The systems arising from space-time finite element discretizations are well-suited for solution by STMG methods. However, most work is based on algebraic multigrid methods [62, 43, 44]. Geometric STMG methods have first been addressed in [34] and later in [30, 39] as well as in the references therein. In terms of the discretization, this work has some similarities to [30], but we take a different approach. We consider discontinuous and continuous discretizations in time for heat and wave equations, and we use a different smoother and focus on more practical aspects of space-time multigrid. Other works use geometric multigrid methods, but only consider the potential of parallelism within one time step [3, 4]. The authors of [37] introduce robust preconditioners for space-time isogeometric analysis of parabolic evolution problems, utilizing a time-parallel multigrid approach with discontinuous variational time discretizations, which we also employ here. The smoother is specifically designed for symmetric saddle point problems and exploits the structure of the operator.

Recently, there has been some contributions towards the all-at-once solution of PDEs leveraging block Toeplitz structures to enhance computational efficiency and parallelizability [47, 38, 31, 64, 15]. In most of these contributions, nonsymmetric block Toeplitz structures are transformed into symmetric systems. The process of symmetrization facilitates the application of more efficient and robust mathematical tools

and algorithms. The aforementioned works primarily examine finite difference discretizations of linear parabolic and hyperbolic problems.

Overall, there is a trend towards leveraging space-time approaches in numerical solution methods for PDEs. This shift is motivated by the need to efficiently address complex problems. As modern processors have reached their clock speed limits, the focus of hardware development is on the increase of the number of processors and the transition to massively parallel computing. To effectively utilize these advances, scalable, efficient, and flexible computational methods are essential. Within this field, one of the central problems that needs to be addressed is the design of performant preconditioners for the arising large linear systems of equations. We argue that multigrid is one of the most promising approaches to addressing these challenges. Then, in the context of STMG methods, the development of efficient smoothers represents another key area of research. The proposed space-time cell-wise ASM smoother turns out to be one of the key features in the design of preconditioners for large linear systems arising from space-time discretizations of PDEs of different type.

The rest of this paper is structured as follows. Section 1.1 introduces the mathematical notation and preliminaries essential for the subsequent discussions. In Section 2 we introduce the space-time finite element discretization, with an emphasis on the continuous and discontinuous approaches to time discretization. In Section 3 we introduce the STMG method including the smoother we use to solve the arising linear systems. The discretization methods are verified through convergence tests, and the performance of the linear solvers is assessed via comprehensive scaling experiments in 4.

## 1.1 Notation

Let  $\Omega \subset \mathbb{R}^d$  for  $d \in \{1, 2, 3\}$  be a bounded domain with boundary  $\partial\Omega = \Gamma_D$  and let  $I = (0, T]$  denote a bounded time interval with final time  $T > 0$ . We split the time interval  $I$  into a sequence of  $N_I$  disjoint subintervals  $I_n = (t_{n-1}, t_n]$ ,  $n = 1, \dots, N_I$  with the time step  $\tau_n := t_n - t_{n-1}$ . By  $\mathcal{T}_\tau$  we refer to the time mesh (or triangulation). For the space discretization, let  $\mathcal{T}_h$  be the quasi-uniform decomposition of  $\Omega$  into quadrilaterals or hexahedra with mesh size  $h > 0$ . Then we denote the space-time tensor product mesh by  $\mathcal{T}_{\tau, h} = \mathcal{T}_h \times \mathcal{T}_\tau$ .

We denote by  $H^1(\Omega)$  the Sobolev space of  $L^2(\Omega)$  functions whose first derivatives are in  $L^2(\Omega)$ . Define  $H := L^2(\Omega)$ ,  $V := H^1(\Omega)$ , and  $V_0 := H_0^1(\Omega)$  as the space of  $H^1$ -functions with vanishing trace on the Dirichlet boundary  $\Gamma_D$ . The  $L^2$ -inner product is  $(\cdot, \cdot)$ , with the norm  $\|\cdot\| := \|\cdot\|_{L^2(\Omega)}$ . For  $J \subseteq [0, T]$  Bochner spaces of  $B$ -valued functions for a Banach space  $B$  are denoted as  $L^2(J; B)$  and  $C(J; B)$ , each equipped with their natural norms. For a Banach space  $B$  and  $k \in \mathbb{N}_0$  we define

$$\mathbb{P}_k(I_n; B) = \left\{ w_{\tau_n} : I_n \rightarrow B \mid w_{\tau_n}(t) = \sum_{j=0}^k W^j t^j \quad \forall t \in I_n, W^j \in B \quad \forall j \right\}. \quad (1)$$

For  $p \in \mathbb{N}$  we define the finite element space that is built on the spatial mesh as

$$\mathcal{V}_h = \left\{ v_h \in C(\bar{\Omega})^d \mid v_h|_K \in \mathbb{Q}_p(K)^d \quad \forall K \in \mathcal{T}_h \right\}, \quad \mathcal{V}_{h,0} = \mathcal{V}_h \cap V_0, \quad (2)$$

where  $\mathbb{Q}_p(K)$  is the space defined by the reference mapping of polynomials on the reference element with maximum degree  $p$  in each variable. For an integer  $k \in \mathbb{N}$  we introduce the space of continuous in time functions

$$\mathcal{X}_\tau^k(B) = \left\{ w \in C(\bar{I}; B) \mid w|_{I_n} \in \mathbb{P}_k(I_n; B) \quad \forall n = 1, \dots, N \right\}. \quad (3)$$

For an integer  $l \in \mathbb{N}_0$  we introduce the space of  $L^2$  in time functions

$$\mathcal{Y}_{\tau, h}^l(B) = \left\{ w \in L^2(I; B) \mid w|_{I_n} \in \mathbb{P}_l(I_n; B) \quad \forall n = 1, \dots, N \right\}. \quad (4)$$

For  $B = \mathcal{V}_h$  we abbreviate the discrete space-time function spaces as follows,

$$\mathcal{X}_{\tau,h}^k = \mathcal{X}_{\tau}^k(\mathcal{V}_h), \quad \mathcal{Y}_{\tau,h}^l = \mathcal{Y}_{\tau,h}^l(\mathcal{V}_h). \quad (5)$$

We express the  $w_{\tau,h}|_{I_n} \in \mathbb{P}_k(I_n; \mathcal{V}_h)$  in terms of space- and time-basis functions  $\phi_j(\mathbf{x})$  and  $\xi_i(t)$

$$w_{\tau,h}|_{I_n}(\mathbf{x}, t) := \sum_{i=1}^{k+1} w_n^i(\mathbf{x}) \xi_{n,i}(t) = \sum_{i=1}^{k+1} \sum_{j=0}^{N_x} w_{n,j}^i \phi_j(\mathbf{x}) \xi_{n,i}(t), \quad \text{for } (\mathbf{x}, t) \in \Omega \times \bar{I}_n. \quad (6)$$

where  $w_{n,i}$  represents the coefficient function to the  $i$ -th time basis function on  $I_n$  and  $w_{n,j}^i$  coefficients to the space-time basis functions. This representation reveals the important tensor-product structure, which is useful for the numerical analysis and the implementation.

## 2 Space-time finite element discretization

We consider the heat and wave equation as a prototypical parabolic and hyperbolic problem. The heat equation with thermal diffusivity  $\rho \in L^2(\mathbb{R})$  is given by

$$\partial_t u - \nabla \cdot (\rho \nabla u) = f, \quad (7)$$

equipped with appropriate initial and boundary conditions. Integrating the strong formulation in space and time and multiplying by space-time test functions yields the global space-time variational form: Find  $u \in W(I) := \{u \in L^2(I; V) \mid \partial_t u \in L^2(I; H)\}$  such that for all  $w \in W_0(I) := \{w \in L^2(I; V_0) \mid \partial_t w \in L^2(I; L)\}$ ,

$$\int_I ((\partial_t u, w) + (\rho \nabla u, \nabla w)) \, dt = \int_I (f, w) \, dt + (u(0), w(0)).$$

The acoustic wave equation with sound speed  $\rho \in L^2(\mathbb{R})$ , written as a first order in time system, is given by

$$\partial_t u - v = 0, \quad \partial_t v - \nabla \cdot (\rho \nabla u) = f, \quad (8)$$

equipped with appropriate initial and boundary conditions. Integrating the strong formulation in space and time and multiplying by space-time test functions yields the global space-time variational form: Find  $(v, u) \in (W(I) \times W(I))$  such that for all  $(\tilde{w}, w) \in W_0(I) \times W_0(I)$ ,

$$\int_I ((\partial_t u, \tilde{w}) - (v, \tilde{w})) \, dt = 0, \quad \int_I ((\partial_t v, w) + (\rho \nabla u, \nabla w)) \, dt = \int_I (f, w) \, dt + (v(0), w(0)).$$

For the discretization in space, let  $\{\phi_j\}_{j=1}^{N_x} \subset \mathcal{V}_h$  denote a nodal Lagrangian basis of  $\mathcal{V}_h$ . The mass and stiffness matrix  $\mathbf{M}_h$  and  $\mathbf{A}_h$  are defined by

$$\mathbf{M}_h := ((\phi_i, \phi_j))_{i,j=1}^{N_x}, \quad \mathbf{A}_h := ((\rho \nabla \phi_i, \nabla \phi_j))_{i,j=1}^{N_x}. \quad (9)$$

Two types of time discretizations are considered:  $DG(k)$ , a discontinuous Galerkin method, and  $CGP(k)$ , a continuous Galerkin-Petrov discretization, both of order  $k$ . The A-stability of the  $CGP(k)$  method for  $k \geq 1$  and the L-stability of the  $DG(k)$  method for  $k \geq 0$  were established in [58] and [36]. We describe these discretization schemes in the following sections.

## 2.1 The discontinuous Galerkin time discretization

We introduce the  $DG(k)$ ,  $k \geq 0$  methods for the space-time discretization, utilizing  $\mathcal{Y}_{\tau,h}^k$  (cf. (5)) for the trial and test spaces. This allows for discontinuities in the trial functions across each subinterval  $I_n$ . For brevity, we assume that the time steps are of uniform size, i. e.  $\tau = \tau_n$  for  $n = 1, \dots, N_T$ . The resulting systems decouple at the endpoints of the subintervals  $I_n$ , facilitating a piecewise solution approach across each interval. For discontinuous functions  $w_\tau(t) \in \mathcal{Y}_{\tau,h}^k$ , we define:

$$w_n^- := \lim_{t \rightarrow t_n^-} w_{\tau,h}(t), \quad w_n^+ := \lim_{t \rightarrow t_n^+} w_{\tau,h}(t), \quad [w_{\tau,h}]_n := w_n^+ - w_n^-. \quad (10)$$

To obtain a time marching problem, we introduce a temporal test basis that is supported on the subintervals  $I_n$ . Let  $\{\xi_i\}_{i=1}^{k+1} \subset \mathbb{P}_k(I_n, \mathbb{R})$  and  $\{\hat{\xi}_i\}_{i=1}^{k+1} \subset \mathbb{P}_k(\hat{I}, \mathbb{R})$ ,  $\hat{I} := [0, 1]$  denote the Lagrangian basis of  $\mathbb{P}_k(I_n, \mathbb{R})$  and  $\mathbb{P}_k(\hat{I}, \mathbb{R})$  w. r. t. the integration points of the  $k + 1$  point Gauss-Radau quadrature. With the affine transformation

$$T_n : \hat{I} \rightarrow I_n, \quad \hat{t} \mapsto t_{n-1} + (t_n - t_{n-1})\hat{t}, \quad (11)$$

the  $i$ th basis function  $\xi_i$  on  $I_n$  is given by the composition of

$$\hat{\xi}_i \circ T_n^{-1} =: \xi_i, \quad (12)$$

for  $i = 1, \dots, k + 1$ . Then, the matrices for the time discretization are given through the weights  $M_h \in \mathbb{R}^{N_t \times N_t}$ ,  $A_\tau \in \mathbb{R}^{N_t \times N_t}$  and  $\alpha \in \mathbb{R}^{N_t}$ , with

$$(M_\tau)_{i,j} := \tau \int_{\hat{I}} \hat{\xi}_j(\hat{t}) \hat{\xi}_i(\hat{t}) d\hat{t}, \quad (A_\tau)_{i,j} := \int_{\hat{I}} \hat{\xi}'_j(\hat{t}) \hat{\xi}_i(\hat{t}) d\hat{t} + \hat{\xi}'_j(1) \hat{\xi}_i(1), \quad \alpha_i := \hat{\xi}'_j(0) \hat{\xi}_i(0), \quad i, j = 1, \dots, N_t, \quad (13)$$

where  $N_t = k + 1$  is the number of temporal degrees of freedom. In the following we directly derive the local subproblems of the time marching problem and then derive subproblems containing multiple time steps. For the derivation of the global space-time variational formulations and the resulting global systems of equations we refer to [40].

### 2.1.1 Discontinuous Galerkin time discretization of the heat equation

Consider the local problem on the interval  $I_n$  where the trajectories  $u_{\tau,h}(t)$  have already been computed for all  $t \in [0, t_{n-1}]$  with initial conditions  $u_{\tau,h}(0) = u_{0,h}$ , where  $u_{0,h} := I_{\mathcal{V}_h} u_0$  denotes the projection of  $v_0 \in V$  onto  $\mathcal{V}_h$ . Given  $u_{\tau,h}(t_{n-1}) \in \mathcal{V}_h$ , the variational problem for the  $DG(k)$  method is formulated as finding  $u_{\tau,h} \in \mathbb{P}_k(I_n; \mathcal{V}_h)$ , such that for all  $w_{\tau,h} \in \mathbb{P}_k(I_n; \mathcal{V}_h)$

$$\int_{I_n} (\partial_t u_{\tau,h}, w_{\tau,h}) + (\nabla u_{\tau,h}, \nabla w_{\tau,h}) dt + ([u_{\tau,h}]_{n-1}, w_{n-1}^+) = \int_{I_n} (f_{\tau,h}, w_{\tau,h}) dt, \quad (14)$$

with  $u_{n-1}^- = u_{\tau,h}|_{t_{n-1}}(t_{n-1})$ . As the trial and test functions  $w_{\tau,h} \in \mathcal{Y}_{\tau,h}^k$  can be discontinuous at interval boundaries, the right and left limits, denoted by  $w_n^+$  and  $w_n^-$ , as defined in (10), are not equal. This gives rise to the jump terms introduced in (10) within the variational formulation (14). They are essential for maintaining the conservation properties and the correct flux balances at the interval boundaries. Upon performing numerical integration, the arising algebraic system in the  $n$ -th time step of the  $CG(p)$ - $DG(k)$  space-time finite element discretization amounts to determining  $\mathbf{u}_n = (\mathbf{u}_n^1, \dots, \mathbf{u}_n^{N_t})^\top$ ,  $\mathbf{u}_n^* \in \mathbb{R}^{N_x}$  such that

$$\underbrace{(M_\tau \otimes A_h + A_\tau \otimes M_h)}_{:=S} \mathbf{u}_n = M_\tau \otimes M_h \mathbf{f}_n + \alpha \otimes M_h \mathbf{u}_{n-1}^{N_t}, \quad (15)$$

where  $\mathbf{f}_n = (\mathbf{f}_n^1, \dots, \mathbf{f}_n^{N_t})^\top$ ,  $\mathbf{f}_{n,j}^i = (f(\mathbf{x}, t_n^q), w_j)$ . Here,  $t_n^q$ ,  $q = 1, \dots, k+1$  is the  $q$ -th point of the Gauss-Radau quadrature rule with  $k+1$  points. In (15), the blocks of  $\mathbf{u}_n$  correspond to the temporal degrees of freedom and the elements of the blocks,  $\mathbf{u}_n^* \in \mathbb{R}^{N_x}$  correspond to the spatial degrees of freedom. Let  $\mathbf{1}_l \in \mathbb{R}^{m \times n}$  be the matrix with entries  $a_{i,j} = \delta_{i,j}$ . Let  $\mathbf{B} := \mathbf{1}_{k+1} \otimes \boldsymbol{\alpha} \otimes \mathbf{M}_h$ . Later we want to apply  $h$ -multigrid in time (we may refer to it as  $\tau$ -multigrid), so we collect consecutive time steps  $n_1, \dots, n_c$  in one system for a  $CG(p) - DG(k)$  space-time finite element discretization. Motivated by [30], similar formulations has also been used in [26]. Using (15) we derive the algebraic system for the solution of multiple time steps at once as

$$\begin{pmatrix} \mathbf{S} & & & & & \\ -\mathbf{B} & \mathbf{S} & & & & \\ & & \ddots & & & \\ & & & \ddots & & \\ & & & & -\mathbf{B} & \mathbf{S} \\ & & & & & -\mathbf{B} & \mathbf{S} \end{pmatrix} \begin{pmatrix} \mathbf{u}_{n_1} \\ \mathbf{u}_{n_2} \\ \vdots \\ \mathbf{u}_{n_{c-1}} \\ \mathbf{u}_{n_c} \end{pmatrix} = \begin{pmatrix} \mathbf{M}_\tau \otimes \mathbf{M}_h \mathbf{f}_{n_1} + \boldsymbol{\alpha} \otimes \mathbf{M}_h \mathbf{u}_{n_1-1}^{N_t} \\ \mathbf{M}_\tau \otimes \mathbf{M}_h \mathbf{f}_{n_2} \\ \vdots \\ \mathbf{M}_\tau \otimes \mathbf{M}_h \mathbf{f}_{n_{c-1}} \\ \mathbf{M}_\tau \otimes \mathbf{M}_h \mathbf{f}_{n_c} \end{pmatrix}. \quad (16)$$

### 2.1.2 Discontinuous Galerkin time discretization of the wave equation

Consider the local problem on the interval  $I_n$  where the trajectories  $u_{\tau,h}(t)$  and  $v_{\tau,h}(t)$  have already been computed for all  $t \in [0, t_{n-1}]$  with initial conditions  $u_{\tau,h}(0) = u_{0,h}$ ,  $v_{\tau,h}(0) = v_{0,h}$ , where  $u_{0,h} := I_{\mathcal{V}_h} u_0$ ,  $v_{0,h} := I_{\mathcal{V}_h} v_0$ . Given  $u_{\tau,h}(t_{n-1}), v_{\tau,h}(t_{n-1}) \in \mathcal{V}_h$ , the variational problem for the  $DG(k)$  method is formulated as finding  $u_{\tau,h}, v_{\tau,h} \in \mathbb{P}_k(I_n; \mathcal{V}_h)$ , such that

$$\begin{aligned} \int_{I_n} (\partial_t u_{\tau,h}, \tilde{w}_{\tau,h}) dt + ([u_{\tau,h}]_{n-1}, \tilde{w}_{n-1}^+) - \int_{I_n} (v_{\tau,h}, \tilde{w}_{\tau,h}) dt &= 0, \\ \int_{I_n} (\partial_t v_{\tau,h}, w_{\tau,h}) dt + ([v_{\tau,h}]_{n-1}, w_{n-1}^+) + \int_{I_n} (\rho \nabla u_{\tau,h}, \nabla w_{\tau,h}) dt &= \int_{I_n} (f, w_{\tau,h}) dt, \end{aligned} \quad (17)$$

for all  $w_{\tau,h}, \tilde{w}_{\tau,h} \in \mathbb{P}_k(I_n; \mathcal{V}_h)$ , with  $u_{n-1}^- = u_{\tau,h}|_{I_{n-1}}(t_{n-1})$ ,  $v_{n-1}^- = v_{\tau,h}|_{I_{n-1}}(t_{n-1})$ . Note the jump terms arising in (17), analogous to (14). Specifically, the jump terms arise for those variables on which a time derivative is present, see [40] for details. Upon numerical integration, the resulting algebraic system in the  $n$ -th time step of the  $CG(p) - DG(k)$  space-time finite element discretization amounts to determining  $\mathbf{u}_n = (\mathbf{u}_n^1, \dots, \mathbf{u}_n^{N_t})^\top$ ,  $\mathbf{v}_n = (\mathbf{v}_n^1, \dots, \mathbf{v}_n^{N_t})^\top$ , where  $\mathbf{u}_n^*, \mathbf{v}_n^* \in \mathbb{R}^{N_x}$ , such that

$$\mathbf{v}_n = \mathbf{M}_\tau^{-1} \mathbf{A}_\tau \mathbf{u}_n - \mathbf{M}_\tau^{-1} \boldsymbol{\alpha} \mathbf{u}_{n-1}^{N_t}, \quad (18a)$$

$$\underbrace{(\mathbf{M}_\tau \otimes \mathbf{A}_h + \mathbf{A}_\tau \mathbf{M}_\tau^{-1} \mathbf{A}_\tau \otimes \mathbf{M}_h)}_{:=\mathbf{S}} \mathbf{u}_n = \mathbf{M}_\tau \otimes \mathbf{M}_h \mathbf{f} + \boldsymbol{\alpha} \otimes \mathbf{M}_h \mathbf{v}_{n-1}^{N_t} + \underbrace{\mathbf{A}_\tau \mathbf{M}_\tau^{-1} \boldsymbol{\alpha}}_{:=\mathbf{D}} \otimes \mathbf{M}_h \mathbf{u}_{n-1}^{N_t}. \quad (18b)$$

In (18a), we observe that the system of equations comprises solely time derivatives. This allows for the condensation of the system, such that we only solve for the displacement  $\mathbf{u}_n$ . The velocity  $\mathbf{v}_n$  is computed by means of simple vector update equations in a second step. To be able to use  $\tau$ -multigrid, we collect consecutive time steps  $n_1, \dots, n_c$  in one system for a  $CG(p) - DG(k)$  space-time finite element discretization. To this end, let  $\mathbf{B} := (\mathbf{M}_\tau)_{k+1, k+1}^{-1} \boldsymbol{\alpha} (\mathbf{A}_\tau)_{k+1, \cdot} \otimes \mathbf{M}_h + \mathbf{D}$ ,  $\mathbf{C} := (\mathbf{M}_\tau)_{k+1, k+1}^{-1} \mathbf{1}_{k+1} \otimes \boldsymbol{\alpha} \otimes \mathbf{M}_h$ . Using (18) we derive the algebraic system for the solution of multiple time steps at once as

$$\begin{pmatrix} \mathbf{S} & & & & & \\ -\mathbf{B} & \mathbf{S} & & & & \\ -\mathbf{C} & -\mathbf{B} & \mathbf{S} & & & \\ & & \ddots & & & \\ & & & \ddots & & \\ & & & & -\mathbf{C} & -\mathbf{B} & \mathbf{S} \\ & & & & & -\mathbf{C} & -\mathbf{B} & \mathbf{S} \end{pmatrix} \begin{pmatrix} \mathbf{u}_{n_1} \\ \mathbf{u}_{n_2} \\ \mathbf{u}_{n_3} \\ \vdots \\ \mathbf{u}_{n_{c-1}} \\ \mathbf{u}_{n_c} \end{pmatrix} = \begin{pmatrix} \mathbf{M}_\tau \otimes \mathbf{M}_h \mathbf{f}_{n_1} + \boldsymbol{\alpha} \otimes \mathbf{M}_h \mathbf{v}_{n_1-1}^{N_t} + \mathbf{D} \mathbf{u}_{n_1-1}^{N_t} \\ \mathbf{M}_\tau \otimes \mathbf{M}_h \mathbf{f}_{n_2} + \mathbf{C} \mathbf{u}_{n_1-1}^{N_t} \\ \mathbf{M}_\tau \otimes \mathbf{M}_h \mathbf{f}_{n_3} \\ \vdots \\ \mathbf{M}_\tau \otimes \mathbf{M}_h \mathbf{f}_{n_{c-1}} \\ \mathbf{M}_\tau \otimes \mathbf{M}_h \mathbf{f}_{n_c} \end{pmatrix}. \quad (19)$$

## 2.2 The continuous Galerkin-Petrov time discretization

Given the continuous time-discrete trial space  $\mathcal{X}_{\tau,h}^k$  (cf. (5)), and the discontinuous time-discrete test space  $\mathcal{Y}_{\tau,h}^{k-1}$ , the method solves local problems on each subinterval  $I_n$  with given initial conditions. This is due to the test functions in  $\mathcal{Y}_{\tau,h}^{k-1}$  having one polynomial degree less than the trial functions, which introduces a system of equations that decouples at  $t_n$  due to the discontinuity of the test functions. The additional degree of freedom in the trial functions is fixed by the continuity of  $\mathcal{X}_{\tau,h}^k$ : We impose a continuity constraint at the left boundary of  $I_n$ , enabling the problem to be solved using a time-marching process. To this end we introduce a temporal test basis that is supported on the subintervals  $I_n$ . Let  $\{\xi_i\}_{i=1}^{k+1} \subset \mathbb{P}_k(I_n, \mathbb{R})$ ,  $\{\hat{\xi}_i\}_{i=1}^{k+1} \subset \mathbb{P}_k(\hat{I}, \mathbb{R})$ ,  $\hat{I} := [0, 1]$  denote the Lagrangian basis of  $\mathbb{P}_k(I_n, \mathbb{R})$ ,  $\mathbb{P}_k(\hat{I}, \mathbb{R})$  w. r. t. the integration points of the  $k+1$  point Gauss-Lobatto quadrature. For the trial space, let  $\{\psi_i\}_{i=1}^k \subset \mathbb{P}_{k-1}(I_n, \mathbb{R})$ ,  $\{\hat{\psi}_i\}_{i=1}^k \subset \mathbb{P}_{k-1}(\hat{I}, \mathbb{R})$  denote the Lagrangian basis of  $\mathbb{P}_{k-1}(I_n, \mathbb{R})$ ,  $\mathbb{P}_{k-1}(\hat{I}, \mathbb{R})$  w. r. t. the last  $k$  integration points of the  $k+1$  point Gauss-Lobatto quadrature.

With the affine transformation (11), the  $i$ th basis function  $\xi_i$  or  $\psi_i$  on  $I_n$  is given by (12). Then, the matrices for the time discretization are given through the weights  $\mathbf{M}_\tau \in \mathbb{R}^{N_t \times N_t}$ ,  $\mathbf{A}_\tau \in \mathbb{R}^{N_t \times N_t}$ ,  $\boldsymbol{\beta} \in \mathbb{R}^{N_t}$  and  $\boldsymbol{\alpha} \in \mathbb{R}^{N_t}$ , with

$$\begin{aligned} (\mathbf{M}_\tau)_{i,j-1} &:= \tau \int_{\hat{I}} \hat{\xi}_j(\hat{t}) \hat{\psi}_i(\hat{t}) \, d\hat{t}, & (\mathbf{A}_\tau)_{i,j-1} &:= \int_{\hat{I}} \hat{\xi}'_j(\hat{t}) \hat{\psi}_i(\hat{t}) \, d\hat{t}, \\ \boldsymbol{\beta}_i &:= \tau \int_{\hat{I}} \hat{\xi}_1(\hat{t}) \hat{\psi}_i(\hat{t}) \, d\hat{t}, & \boldsymbol{\alpha}_i &:= \int_{\hat{I}} \hat{\xi}'_1(\hat{t}) \hat{\psi}_i(\hat{t}) \, d\hat{t}, \quad i = 1, \dots, N_t, \quad j = 2, \dots, N_t + 1 \end{aligned} \quad (20)$$

where  $N_t = k$  is the number of temporal degrees of freedom in the algebraic system we derive next, as we already separated the weights associated to the degree of freedom fixed by the continuity constraints into  $\boldsymbol{\beta}$  and  $\boldsymbol{\alpha}$ .

### 2.2.1 Continuous Galerkin-Petrov time discretization of the heat equation

Consider the local problem on the interval  $I_n$  where the trajectories  $u_{\tau,h}(t)$  have already been computed for all  $t \in [0, t_{n-1}]$  with initial conditions  $u_{\tau,h}(0) = u_{0,h}$ , where  $u_{0,h} := I_{\mathcal{V}_h} u_0$  denotes the interpolation of  $u_0 \in H$  onto  $\mathcal{V}_h$ . Given  $u_{\tau,h}(t_{n-1}) \in \mathcal{V}_h$ , the variational problem for the CGP( $k$ ) method is formulated as finding  $u_{\tau,h} \in \mathbb{P}_k(I_n; \mathcal{V}_h)$ , such that for all  $w_{\tau,h} \in \mathbb{P}_{k-1}(I_n; \mathcal{V}_h)$

$$\int_{I_n} (\partial_t u_{\tau,h}, w_{\tau,h}) + (\nabla u_{\tau,h}, \nabla w_{\tau,h}) \, dt = \int_{I_n} (f, w_{\tau,h}) \, dt, \quad (21)$$

with the continuity constraint  $u_{n-1}^- = u_{\tau,h}|_{I_{n-1}}(t_{n-1})$ . Upon numerical integration (cf. [40]), the algebraic system that arises in the  $n$ -th time step of the CG( $p$ ) – CGP( $k$ ) space-time finite element discretization amounts to determining  $\mathbf{u}_n = (\mathbf{u}_n^1, \dots, \mathbf{u}_n^{N_t})^\top$ , where  $\mathbf{u}_n^* \in \mathbb{R}^{N_x}$  such that

$$\underbrace{(\mathbf{M}_\tau \otimes \mathbf{A}_h + \mathbf{A}_\tau \otimes \mathbf{M}_h)}_{:=\mathbf{S}} \mathbf{u}_n = \mathbf{M}_\tau \otimes \mathbf{M}_h \mathbf{f}_n - \boldsymbol{\beta} \otimes \mathbf{M}_h \mathbf{f}_{n-1}^{N_t} + \underbrace{(\boldsymbol{\beta} \otimes \mathbf{A}_h + \boldsymbol{\alpha} \otimes \mathbf{M}_h)}_{:=\mathbf{b}} \mathbf{u}_{n-1}^{N_t} \quad (22)$$

where  $\mathbf{f}_n = (\mathbf{f}_n^1, \dots, \mathbf{f}_n^{N_t})^\top$ ,  $\mathbf{f}_{n,j}^i = (f(\mathbf{x}, t_n^q), w_j)$ . The points  $t_n^q$ ,  $q = 1, \dots, k$  are the  $q+1$ -th nodes of the Gauss-Lobatto quadrature rule with  $k+1$  points. Note that by this choice of quadrature rule the continuity constraint can be written as  $\mathbf{u}_{n-1}^{N_t} = \mathbf{u}_n^0$ . Here,  $\mathbf{u}_n^0$  is the temporal degree of freedom at the first Gauss-Lobatto quadrature point, with the zero index indicating that it acts algebraically like an initial condition. Let  $\mathbf{B} := \mathbf{1}_k \otimes \mathbf{b}$ . Analogous to the DG time stepping, we collect consecutive time steps

$n_1, \dots, n_c$  in one system for a  $CG(p) - CGP(k)$  space-time finite element discretization. Using (22) we derive the algebraic system for the solution of multiple time steps at once as

$$\begin{pmatrix} S & & & & \\ -B & S & & & \\ & & \ddots & & \\ & & & -B & S \\ & & & -B & S \end{pmatrix} \begin{pmatrix} \mathbf{u}_{n_1} \\ \mathbf{u}_{n_2} \\ \vdots \\ \mathbf{u}_{n_{c-1}} \\ \mathbf{u}_{n_c} \end{pmatrix} = \begin{pmatrix} \mathbf{M}_\tau \otimes \mathbf{M}_h \mathbf{f}_{n_1} - \boldsymbol{\beta} \otimes \mathbf{M}_h \mathbf{f}_{n_{1-1}}^{N_t} + \mathbf{b} \mathbf{u}_{n_{1-1}}^{N_t} \\ \mathbf{M}_\tau \otimes \mathbf{M}_h \mathbf{f}_{n_2} - \boldsymbol{\beta} \otimes \mathbf{M}_h \mathbf{f}_{n_1}^{N_t} \\ \vdots \\ \mathbf{M}_\tau \otimes \mathbf{M}_h \mathbf{f}_{n_{c-1}} - \boldsymbol{\beta} \otimes \mathbf{M}_h \mathbf{f}_{n_{c-2}}^{N_t} \\ \mathbf{M}_\tau \otimes \mathbf{M}_h \mathbf{f}_{n_c} - \boldsymbol{\beta} \otimes \mathbf{M}_h \mathbf{f}_{n_{c-1}}^{N_t} \end{pmatrix}. \quad (23)$$

### 2.2.2 Continuous Galerkin-Petrov time discretization of the wave equation

Consider the local problem on the interval  $I_n$  where the trajectories  $u_{\tau,h}(t)$  and  $v_{\tau,h}(t)$  have already been computed for all  $t \in [0, t_{n-1}]$  with initial conditions  $u_{\tau,h}(0) = u_{0,h}$ ,  $v_{\tau,h}(0) = v_{0,h}$ , where  $u_{0,h} := I_{\mathcal{V}_h} u_0$ ,  $v_{0,h} := I_{\mathcal{V}_h} v_0$ . Given  $u_{\tau,h}(t_{n-1}), v_{\tau,h}(t_{n-1}) \in \mathcal{V}_h$ , the variational problem for the DG( $k$ ) method is formulated as finding  $u_{\tau,h}, v_{\tau,h} \in \mathbb{P}_{k-1}(I_n; \mathcal{V}_h)$ , such that

$$\int_{I_n} (\partial_t u_{\tau,h}, w_{\tau,h}) - (v_{\tau,h}, w_{\tau,h}) \, dt = 0, \quad \int_{I_n} (\partial_t v_{\tau,h}, w_{\tau,h}) + (\rho \nabla u_{\tau,h}, \nabla w_{\tau,h}) \, dt = \int_{I_n} (f, w_{\tau,h}) \, dt, \quad (24)$$

for all  $w_{\tau,h}, \tilde{w}_{\tau,h} \in \mathbb{P}_k(I_n; \mathcal{V}_h)$ , with  $u_{n-1}^- = u_{\tau,h}|_{I_{n-1}}(t_{n-1}), v_{n-1}^- = v_{\tau,h}|_{I_{n-1}}(t_{n-1})$ . Upon performing numerical integration, the arising algebraic system in the  $n$ -th time step of the  $CG(p) - CGP(k)$  space-time finite element discretization amounts to determining  $\mathbf{u}_n = (\mathbf{u}_n^1, \dots, \mathbf{u}_n^{N_t})^\top, \mathbf{v}_n = (\mathbf{v}_n^1, \dots, \mathbf{v}_n^{N_t})^\top, \mathbf{u}_n^*, \mathbf{v}_n^* \in \mathbb{R}^{N_x}$  such that

$$\mathbf{v}_n = \mathbf{M}_\tau^{-1} \mathbf{A}_\tau \mathbf{u}_n - \mathbf{M}_\tau^{-1} \boldsymbol{\alpha} \mathbf{u}_{n-1}^{N_t} + \mathbf{M}_\tau^{-1} \boldsymbol{\beta} \mathbf{v}_{n-1}^{N_t}, \quad (25a)$$

$$\underbrace{(\mathbf{M}_\tau \otimes \mathbf{A}_h + \mathbf{A}_\tau \mathbf{M}_\tau^{-1} \mathbf{A}_\tau \otimes \mathbf{M}_h)}_{:=S} \mathbf{u}_n = \mathbf{M}_\tau \otimes \mathbf{M}_h \mathbf{f} - \boldsymbol{\beta} \otimes \mathbf{M}_h \mathbf{f}_{n-1}^{N_t} + (\boldsymbol{\beta} \otimes \mathbf{A}_h + \mathbf{A}_\tau \mathbf{M}_\tau^{-1} \boldsymbol{\alpha} \otimes \mathbf{M}_h) \mathbf{u}_{n-1}^{N_t} + (\boldsymbol{\alpha} - \mathbf{A}_\tau \mathbf{M}_\tau^{-1} \boldsymbol{\beta}) \otimes \mathbf{M}_h \mathbf{v}_{n-1}^{N_t}. \quad (25b)$$

Analogous to the DG time stepping, we condense the system and compute  $\mathbf{v}_n$  by vector update equations and only solve for the displacement  $\mathbf{u}_n$ . We further collect consecutive time steps  $n_1, \dots, n_c$  in one system for a  $CG(p) - CGP(k)$  space-time finite element discretization of the wave equation. The auxiliary variable  $\mathbf{v}_n$  complicates the system because it is defined recursively by (25a) and depends on the past solution. As for the discontinuous time stepping, this recurrence introduces additional terms in the matrix blocks. Due to the continuity constraints on both variables, the system becomes significantly more complex, at least if we don't introduce higher order derivatives and still want to solve for  $\mathbf{v}$  through vector updates. On the right hand side of (25b) we observe that, in order to derive the system for the solution of multiple time steps at once, we need an equation for the initial value  $\mathbf{v}_{l-1}^{N_t}$  on each interval  $I_l$  for  $l \in \{n_2, \dots, n_c\}$ . Note that we can see in (26), for  $l = n_1$ , we simply recover (25b) and  $\mathbf{v}_{n_{1-1}}^{N_t}$  is known from previous computations. From (25a) we observe that, in contrast to the discontinuous time discretization, the initial value  $\mathbf{v}_{l-1}^{N_t}$ ,  $l \in \{n_2, \dots, n_c\}$  cannot be expressed solely in terms of the displacement variable. For instance, considering (25b) for  $n = n_2$ , we see that we need to replace  $\mathbf{v}_{n_1}^{N_t}$  on the right hand side by deriving an equation for  $\mathbf{v}_{n_1}^{N_t}$  in terms of the variables  $\mathbf{u}_{n_1}$  and  $\mathbf{v}_{n_{1-1}}$ . Doing this by using the auxiliary



differential equation (25a) and iterating this process for all time steps  $n_2, \dots, n_c$ , we get the algebraic system for the solution of multiple time steps at once as

$$\begin{pmatrix} S & & & & \\ -B + E_{2,1} & S & & & \\ E_{3,1} & -B + E_{3,2} & S & & \\ \vdots & \vdots & \ddots & \ddots & \\ \vdots & \ddots & -B + E_{n_c-1, n_c-2} & S & \\ E_{n_c,1} & E_{n_c,2} & \dots & -B + E_{n_c, n_c-1} & S \end{pmatrix} \begin{pmatrix} \mathbf{u}_{n_1} \\ \mathbf{u}_{n_2} \\ \mathbf{u}_{n_3} \\ \vdots \\ \mathbf{u}_{n_{c-1}} \\ \mathbf{u}_{n_c} \end{pmatrix} = F \quad (26a)$$

$$F = \begin{pmatrix} M_\tau \otimes M_h f_{n_1} - \beta \otimes M_h f_{n_1-1}^{N_t} + \beta \otimes A_h u_{n_1-1}^{N_t} + A_\tau M_\tau^{-1} \alpha \otimes M_h u_{n_1-1}^{N_t} + \alpha_{A_\tau} \otimes M_h v_{n_1-1}^{N_t} \\ M_\tau \otimes M_h f_{n_2} - \beta \otimes M_h f_{n_1}^{N_t} - z_{M_\tau} \alpha_{A_\tau} \otimes M_h u_{n_1-1}^{N_t} - g_{M_\tau} \alpha_{A_\tau} \otimes M_h v_{n_1-1}^{N_t} \\ M_\tau \otimes M_h f_{n_3} - \beta \otimes M_h f_{n_2}^{N_t} - z_{M_\tau} g_{M_\tau} \alpha_{A_\tau} \otimes M_h u_{n_1-1}^{N_t} - g_{M_\tau}^2 \alpha_{A_\tau} \otimes M_h v_{n_1-1}^{N_t} \\ \vdots \\ M_\tau \otimes M_h f_{n_{c-1}} - \beta \otimes M_h f_{n_{c-2}}^{N_t} - z_{M_\tau} g_{M_\tau}^{n_c-3} \alpha_{A_\tau} \otimes M_h u_{n_1-1}^{N_t} - g_{M_\tau}^{n_c-2} \alpha_{A_\tau} \otimes M_h v_{n_1-1}^{N_t} \\ M_\tau \otimes M_h f_{n_c} - \beta \otimes M_h f_{n_{c-1}}^{N_t} - z_{M_\tau} g_{M_\tau}^{n_c-2} \alpha_{A_\tau} \otimes M_h u_{n_1-1}^{N_t} - g_{M_\tau}^{n_c-1} \alpha_{A_\tau} \otimes M_h v_{n_1-1}^{N_t} \end{pmatrix} \quad (26b)$$

where we used the notation  $\alpha_{A_\tau} = \alpha - A_\tau M_\tau^{-1} \beta$ ,  $g_{M_\tau} = \beta_k (M_\tau)_{k,k}^{-1}$  and  $z_{M_\tau} = \alpha_k (M_\tau)_{k,k}^{-1}$  and

$$B := \mathbf{1}_k \otimes A_\tau M_\tau^{-1} \alpha \otimes M_h + \mathbf{1}_k \otimes \beta \otimes A_h, \quad (27a)$$

$$E_{i,j} := -C_{i,j} + D_{i,j}. \quad (27b)$$

Here,

$$C_{i,j} := \frac{g_{M_\tau}^{i-j-1}}{(M_\tau)_{k,k}} \alpha_{A_\tau} (A_\tau)_{k,*}, \quad D_{i,j} := \begin{cases} \mathbf{1}_k \otimes g_{M_\tau}^{i-j-2} z_{M_\tau} \alpha_{A_\tau}, & i > 2i - 1 > j \\ 0 & \text{otherwise} \end{cases}, \quad (27c)$$

where  $(A_\tau)_{k,*}$  is the  $k$ th row of  $A_\tau$ .

### 3 Space-time multigrid method

We present the space-time multigrid method to solve the space-time systems (16), (19), (23) and (26). We write the linear systems associated to these problems as

$$S\mathbf{u} = f. \quad (28)$$

To build the hierarchical sequence of space-time meshes  $\{\mathcal{T}_{\tau,h}^l\}_{l=0}^L$ , we only coarsen either in space or in time, as sketched in Figure 1. Of course the reduction in degrees of freedom on each level makes space-time coarsening particularly appealing. Although it is practically feasible, it is challenging in the parallel in time context, as observed for instance in [2]. In [13] the authors derive a CFL-type condition, which ensures convergence with space-time coarsening for a one-dimensional STMG method for finite differences discretizations of the heat equation. Our current investigation is focused on the computational aspects of the proposed method and the efficacy of its implementation. Consequently, the exploration of space-time coarsening techniques is not included in this study and is subject to future work. The extension within our code is straightforward. Analogous to the notion of  $h$  and  $p$  multigrid we denote the same things in time by  $\tau$  and  $k$  multigrid within this paper. Both modes are implemented in our code.

Each level of the space-time multigrid hierarchy is associated to a system of linear equations denoted by  $S_l \mathbf{u}_l = f_l$ . The finest level is associated to the original problem (28). We apply the multigrid in a  $V$ -cycle with a space-time cell-based ASM smoother as preconditioner of GMRES.

### 3.1 Multigrid algorithm

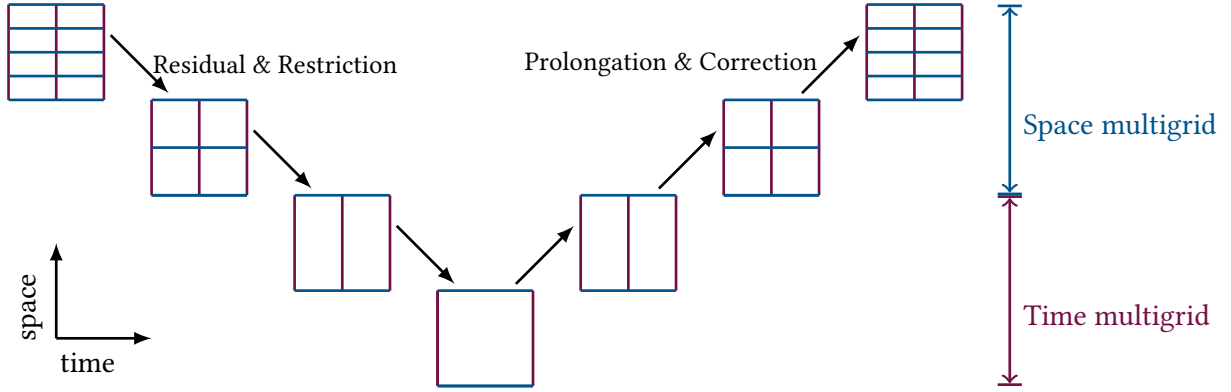


**Figure 1:** A sketch of the STMG method, see also Algorithm 1. The corrections are transferred by the prolongation operators and the residual is transferred by the restriction operators. On each level the error is *smoothed* by a single iteration of the additive Schwarz smoother. The preferred coarsening strategy, which is then used in Algorithm 2, is first in space and then in time.

Space-time multigrid methods expand upon the classical multigrid approach by incorporating space and time dimensions into the grid coarsening process (cf. Figure 1). The objective of this extension is to efficiently solve large-scale partial differential equations by performing coarsening and refinement across space and time dimensions. These methods are of particular interest when spatial parallelism saturates. To gain further parallelization potential, the sizes of the subproblems in every time step are increased by batching multiple time steps in one. Further, when high order discretizations are employed on problems with large coarse problems, temporal multigrid is useful for reducing the size of the coarse problem. For an introduction and more detailed discussion of the geometric multigrid method, we refer to [33, 11, 66, 67].

---

**Algorithm 1:** Space-time multigrid algorithm for problems discretized with space-time finite elements (28). Note the recursive call, which corresponds to a V-cycle.

---

```

1 function Multigrid( $l, \mathcal{S}_l, f_l, \mathbf{u}_l$ )
2   Pre-smooth  $\mathbf{u}_l$  with  $\nu_1$  iterations of a smoother;
3   Compute and restrict residual  $\mathbf{r}_{l-1} = \mathcal{R}_l(f_l - \mathcal{S}_l \mathbf{u}_l)$ ;
4   if  $l$  is the coarsest level then
5     | Solve  $\mathcal{S}_l \mathbf{u}_l = f_l$ ;
6   else
7     |  $\mathbf{e}_{l-1} = \text{Multigrid}(l-1, \mathcal{S}_{l-1}, \mathbf{r}_{l-1}, \mathbf{0})$ ;
8   end
9   Prolongate and correct  $\mathbf{u}_l = \mathbf{u}_l + \mathcal{P}_l \mathbf{e}_{l-1}$ ;
10  Post-smooth  $\mathbf{u}_l$  with  $\nu_2$  iterations of a smoother;
11 end

```

---

The computational complexity of a space-time multigrid cycle (cf. Algorithm 1) is similar to that of multigrid cycles that focus only on spatial coarsening. In the case of spatial coarsening, the number of grid points is reduced by a factor of  $2^d$  at each level, where  $d$  is the spatial dimension. Similar to a one-dimensional spatial coarsening, the number of time steps is halved at each coarsening level. For polynomial multigrid the coarsening factor is derived analogously, depending on the ratio between the polynomial degrees on each level.

In the previous section, we have already formulated the linear systems, that arise from the discretization. For the evaluation of operators we utilize matrix-free methods, where the system matrix is not explicitly formed and stored and exploit the tensor product structure for the efficient evaluation of finite element operators by decomposing multidimensional into one-dimensional operations [41]. In matrix-free methods the matrix-vector product  $\mathbf{y} = \mathbf{S}\mathbf{u}$  is computed directly through local operations and mappings from local to global degrees of freedom:

$$\mathbf{S} = \sum_{c=1}^{n_c} \mathbf{P}_{c, \text{loc-glob}}^T \mathbf{S}_c \mathbf{P}_{c, \text{loc-glob}},$$

where  $\mathbf{P}_{c, \text{loc-glob}}$  maps local degrees of freedom to global indices, and  $\mathbf{S}_c$  is defined by the relation  $\mathbf{S}_c = \mathbf{B}_c^T \mathbf{D}_c \mathbf{B}_c$ . If  $\mathbf{S}$  is a stiffness matrix,  $\mathbf{B}_c$  represents the gradients of shape functions, and  $\mathbf{D}_c$  is a diagonal matrix containing quadrature weights and coefficients. The integrals are evaluated on-the-fly. The sum factorization reduces the computational complexity from  $O(p^{2d})$  to  $O(dp^2)$ , making it significantly more efficient for high-dimensional and high-degree polynomial problems.

The sum-factorization allows for the fast evaluation by the transformation of multi-dimensional operations into sequences of one-dimensional operations and reduces the computational complexity from  $\mathcal{O}(n_{1D}^{2d})$  to  $\mathcal{O}(dn_{1D}^{d+1})$ , where  $n_{1D}$  is the number of degrees of freedom in one spatial direction. Specifically, the local matrix-vector product is represented as

$$\mathbf{S}_c \cdot \mathbf{u}_c = \mathbf{B}_c^T (\mathbf{D}_c (\mathbf{B}_c \cdot \mathbf{u}_c)),$$

with the evaluation of three matrix-vector products, as indicated by the braces, which results in the reduced computational complexity. These techniques are employed for matrix-vector products with the stiffness matrix  $\mathbf{A}_h$  and the mass matrix  $\mathbf{M}_h$  in the space-time systems (16), (19), (23) and (26). The temporal matrices on the other hand are precomputed and stored as full matrices for each subproblem. As they are small and  $N_t \ll N_x$ , this is reasonable and efficient in the current implementation. Moreover, one can evaluate  $(\mathbf{M}_\tau \otimes \mathbf{A}_h + \mathbf{A}_\tau \otimes \mathbf{M}_h)\mathbf{u}$  as  $\mathbf{M}_\tau(\mathbf{A}_h \otimes \mathbf{u}) + \mathbf{A}_\tau(\mathbf{M}_h \otimes \mathbf{u})$ , i. e. calculating  $\mathbf{A}_h \mathbf{u}^i$  and  $\mathbf{M}_h \mathbf{u}^i$  once for each  $i = 1, \dots, N_t$  and reusing it for the multiplication with the temporal matrices throughout the operator evaluation. This is used analogously for other Kronecker products in (16), (19), (23) and (26). By batching multiple time steps into one, the implementation allows for  $N_t$  to become very large. In this case, we plan to extend our implementation to be able to store the temporal matrices as sparse matrices. Here, we keep  $N_t$  at moderate sizes, where this does not pay off yet.

The implementation of the STMG method is based on the geometric multigrid method implemented in deal.II [50]. The only remaining task is to define the transfer and smoothing operators.

### 3.2 Grid transfer

---

**Algorithm 2:** Algorithm to construct space-time multigrid transfers in a multilevel system.

---

**Result:** Space-time multigrid transfer operators

```

1 for  $\ell \leftarrow 0$  to  $L$  do
2   if  $mgType[\ell] == space$  then
3     |   setup space transfers and transfer operators  $\mathcal{R}_\ell, \mathcal{P}_\ell$ ;
4   else
5     |   setup time transfer operators  $\mathcal{R}_\ell, \mathcal{P}_\ell$ ;
6     |   if  $mgType[\ell] == k$ -multigrid then
7     |     |    $r = r - 1$ ;
8     |     |   else if  $mgType[\ell] == \tau$ -multigrid then
9     |     |     |    $timesteps / = 2$ ;
10 end
```

---

The definition of the prolongation operator depends on the coarsening strategy employed at each grid level, as specified by Algorithm 2. For temporal and spatial coarsening, the standard  $L^2$ -projection is applied by the prolongation operators for  $p$  or  $k$  and  $h$  or  $\tau$ -multigrid methods. For a detailed description and performance engineering of the spatial transfers we refer to [50]. For the temporal transfers, in the context of discontinuous Galerkin time discretization, implementing the projections is straightforward. Continuous time discretizations pose a challenge due to the continuity constraints imposed due to the Galerkin-Petrov method. In particular, the first temporal degree of freedom  $\mathbf{u}_n^0$  for each local subproblem on interval  $I_n$  is determined by the continuity constraint  $\mathbf{u}_n^0 = \mathbf{u}_{n-1}^{N_t}$  (cf. Section 2.2.1) and is therefore considered a constrained degree of freedom. As a result, the residuals with respect to this degree of freedom are zero, allowing us to omit them in the transfers of the residuals in the multigrid method. Of course  $\mathbf{u}_n^0$  is accounted for by the problem on  $I_{n-1}$ , where  $\mathbf{u}_{n-1}^{N_t}$  is an unknown in the local linear system. To efficiently implement the temporal transfers, we exploit the tensor product structure inherent in the discretization. Then, the spatial prolongation  $\mathcal{P}_l^h$  applied to the block vector  $\mathbf{u}_l$  is represented by the tensor product  $\mathcal{P}_l^h \otimes \mathbf{u}_l$  and the temporal prolongation is represented by  $\mathcal{P}_l^\tau \mathbf{u}_l$ .

Similarly, the choice of the restriction operator is influenced by the selected coarsening strategy. Typically, the restriction operator is defined as the adjoint of the prolongation operator. Our implementation provides an option to compute the restrictions using  $L^2$ -projections. However, this approach negates the desirable property of maintaining adjoint symmetry between the operators. In practice, both methods have demonstrated comparable performance. Therefore, we maintain the definition of the restriction operator as the adjoint of the prolongation operator throughout this paper. Analogous to the prolongation, the spatial restriction  $\mathcal{R}_l^h$  is given by  $\mathcal{R}_l^h \otimes \mathbf{u}_l = (\mathcal{P}_l^h)^\top \otimes \mathbf{u}_l$  and the temporal restriction  $\mathcal{R}_l^\tau$  is given by  $\mathcal{R}_l^\tau \mathbf{u}_l = (\mathcal{P}_l^\tau)^\top \mathbf{u}_l$ .

### 3.3 Space-time additive Schwarz smoother

The smoothing that preceded the restrictions is usually a simple iteration that approximates the solution of the linear system, i. e.

$$\text{smoother}_l(\mathcal{S}_l, f_l) \approx \mathcal{S}_l^{-1} f_l,$$

and aims to quickly reduce all high frequency components of the residual  $f_l - \mathcal{S}_l \mathbf{u}_l$ . If the residual is reduced at a rate that is constant across all levels  $l$ , then the geometric multigrid method achieves the optimal complexity  $O(N)$ . In our implementation we use a space-time cell wise ASM smoother. The blocks of the ASM consist of all degrees of freedom of a space-time element, which are solved with an inner direct solver. The block size of the ASM is then  $k(p+1)^d$  for the  $CG(k) - CGP(k)$  method and  $(k+1)(p+1)^d$  for the  $CG(k) - DG(k)$  method. The idea of the smoother is to solve small subproblems directly and to replace the inverse of  $\mathcal{S}_l^{-1}$  by

$$\text{smoother}_l(\mathcal{S}_l, f_l) = \left( \sum_{T \in \mathcal{T}_{\tau,h}^l} \mathbf{R}_T^T [\mathbf{R}_T \mathcal{S}_l \mathbf{R}_T^T]^{-1} \mathbf{R}_T \right) f_l \quad (29)$$

where  $\mathbf{R}_T$  is the restriction to those nodes that belong to a space-time mesh element  $T \in \mathcal{T}_{\tau,h}^l$  and  $\mathbf{R}_T^T$  is its transpose. This smoother is computationally expensive and the application on each cell is of complexity

$$O(k^2(p+1)^{2d}) \quad \text{and} \quad O((k+1)^2(p+1)^{2d}), \quad (30)$$

for  $CG(k)$ - $CGP(k)$  and  $CG(k)$ - $DG(k)$  discretizations. With a relaxation parameter  $\omega_l \in (0, 1)$ , an iteration of the smoother (cf. Algorithm 1, line 1 and 9) is then given by

$$\text{Smoother}(\mathcal{S}_l, f_l, \mathbf{u}_l) = \mathbf{u}_l + \omega_l \text{smoother}_l(\mathcal{S}_l, f_l - \mathcal{S}_l \mathbf{u}_l). \quad (31)$$

We note that our current implementation of the space-time ASM smoother does only partially take advantage of the block structure arising from the tensor-product space-time finite elements. We only exploit the block structure to prevent the assembly of the full system matrix. Future work will focus on leveraging these block patterns to improve smoother efficiency and solver scalability.

## 4 Numerical experiments

We evaluate the STMG method when applied to parabolic and hyperbolic PDEs. The evaluation includes numerical convergence tests and two examples of inhomogeneous coefficients. The investigation focuses on the performance and parallel scaling of the algebraic solver, as well as its robustness with respect to discretization order, mesh refinement, and mesh structure. The tests are run on an HPC cluster (HSUper at HSU) with 571 nodes, each with 2 Intel Xeon Platinum 8360Y CPUs and 256 GB RAM. The processors have 36 cores each.

For the solution of the arising algebraic systems we use the STMG method developed in this paper as a preconditioner with a GMRES method. The STMG method (cf. Section 3.1) is employed with a single V-cycle for every GMRES iteration. In the STMG method we use the space-time cell-based ASM smoother presented in Section 3.3. The implementation is based on the geometric multigrid method implemented in deal.II [50]. Evaluations of the linear operator  $S$  are performed using the matrix-free infrastructure described in [41]. In all numerical experiments, the stopping criterion for the GMRES iterations is an absolute residual smaller than  $1 \times 10^{-12}$  (Section 4.1) or  $1 \times 10^{-10}$  (Section 4.2) or a reduction of the initial residual by a factor of  $1 \times 10^{-12}$ . The numerical methods are only tested for the  $p = k$  case, i. e. we consider the  $CG(k)$ - $CGP(k)$  and the  $CG(k)$ - $DG(k)$  method. The relaxation parameter  $\omega_l$  in (31) is determined based on the minimal and maximal eigenvalues  $\lambda_{l,\min}$ ,  $\lambda_{l,\max}$  on each level by

$$\omega_l = \frac{2}{\lambda_{l,\max} + \lambda_{l,\min}}. \quad (32)$$

The eigenvalues are estimated according to [49, Section 2.2]. The relaxation parameter is optimal for iterative methods applied to symmetric positive definite matrices, such as the Jacobi method. We adopt it here as a sensible choice. In the numerical experiments it can lead to improved convergence rates and performs at least as well as  $\omega_l = 1$ .

### 4.1 Numerical convergence tests

We verify the space-time finite element methods for the heat and wave equation for the  $CG(k)$ - $CGP(k)$  and the  $CG(k)$ - $DG(k)$  method. In order to be able to validate the numerical methods by calculating the experimental orders of convergence (EOC), we prescribe the same solution

$$u(\mathbf{x}, t) = \sin(2\pi ft) \sin(2\pi fx) \sin(2\pi fy) \sin(2\pi fz), \quad (33)$$

with  $f = 2$  for the heat and the wave equation. We consider this 3D test case in the space-time domain  $\Omega \times I = [0, 1]^3 \times [0, 1]$ . The initial time mesh  $\mathcal{T}_\tau$  consists of the twice uniformly refined interval  $I$ , while the initial spatial mesh  $\mathcal{T}_h$  consists of the once uniformly refined hypercube  $\Omega$ . The thermal diffusivity and sound speed are set to 1. All convergence tests were performed on 96 nodes of the HPC cluster. In all tests we perform a STMG method with at least one level in space and time. The convergence rate is not affected by the number of time steps that are batched into a single system. We therefore don't report the convergence rates for different space-time multigrid sequences. We report the influence of different space-time multigrid sequences on the performance of the iteration count. The number of smoothing steps is set to  $n_{\text{smooth}} = 1$ .

### 4.1.1 Convergence tests of the heat equation

We perform convergence tests for the systems (16) and (23). We evaluate the performance of STMG on a Cartesian grid. To ensure effectiveness of STMG on complex spatial domains, we also consider perturbed meshes. For this, we apply a random displacement to all vertices of the grid. The direction of movement of each vertex is randomly generated, while the length of the shift vector is set to 0.15 times the minimal length of the edges adjacent to this vertex. The convergence test has homogeneous Dirichlet boundary conditions. We study the errors  $e_u = u(x, t) - u_{\tau, h}(x, t)$  in the norms given by

$$\|e_u\|_{L^\infty(L^\infty)} = \max_{t \in I} \left( \sup_{\Omega} \|u\|_{\infty} \right), \quad \|e_u\|_{L^2(L^2)} = \left( \int_I \int_{\Omega} |e_u|^2 dx dt \right)^{\frac{1}{2}}. \quad (34)$$

We abbreviate the error quantity  $\|e_u\|_{L^\infty(L^2)}$  by  $L^\infty - L^2(u)$  and analogously for the other norms. We verify the accuracy of the  $CG(k) - DG(k)$  and  $CG(k) - CGP(k)$  methods for  $p = k$ ,  $k \in \{2, 3, 4, 5\}$ . In Figure 2 we observe that the optimal orders of convergence are achieved for Cartesian and perturbed meshes for  $CG(k) - DG(k)$  discretizations.

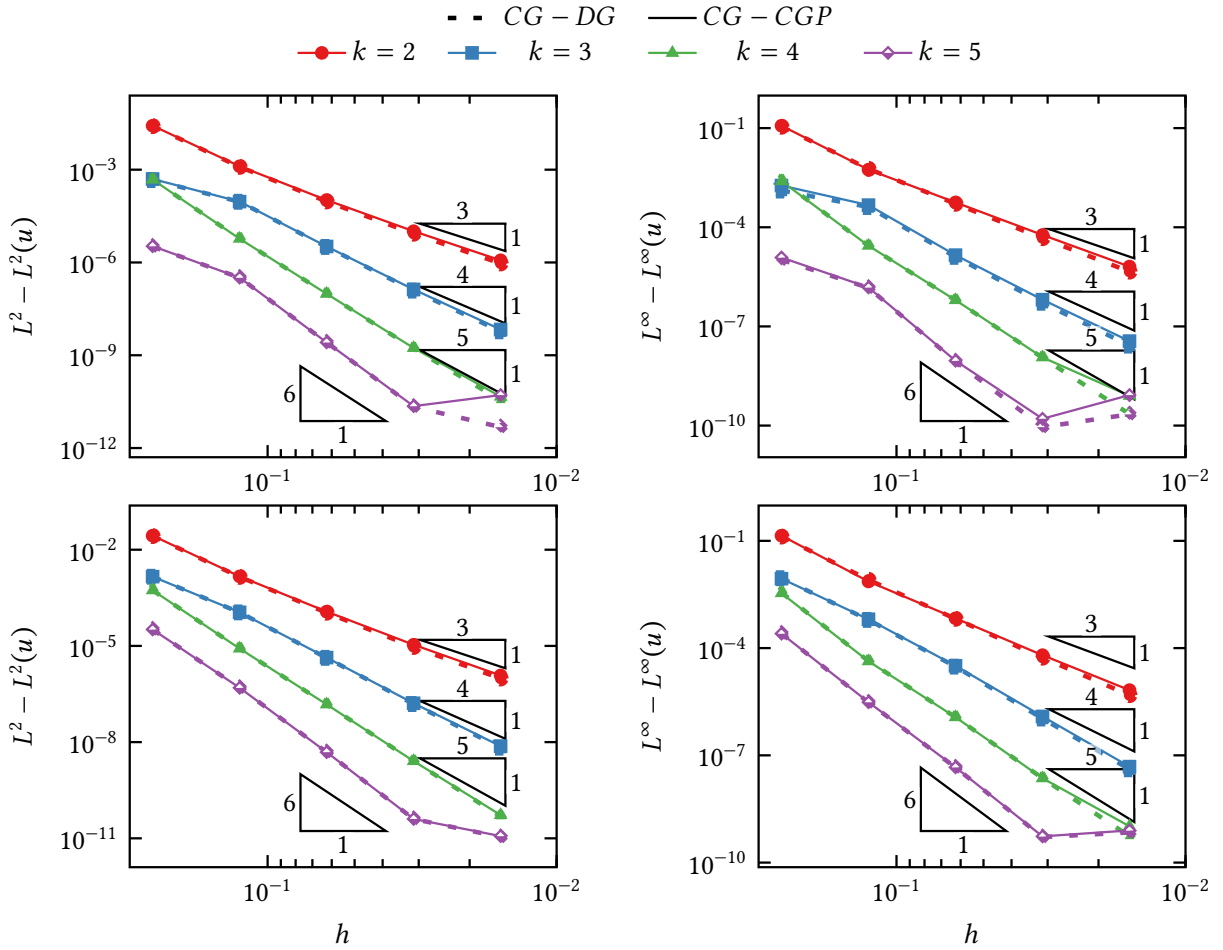


**Figure 2:** Calculated errors for  $u$  for different orders of convergence on Cartesian meshes (top row) and perturbed meshes (bottom row) for  $CG(k) - DG(k)$  discretizations of the heat equation. The expected orders of convergence  $k + 1$ , represented by the triangles, match with the experimental orders.

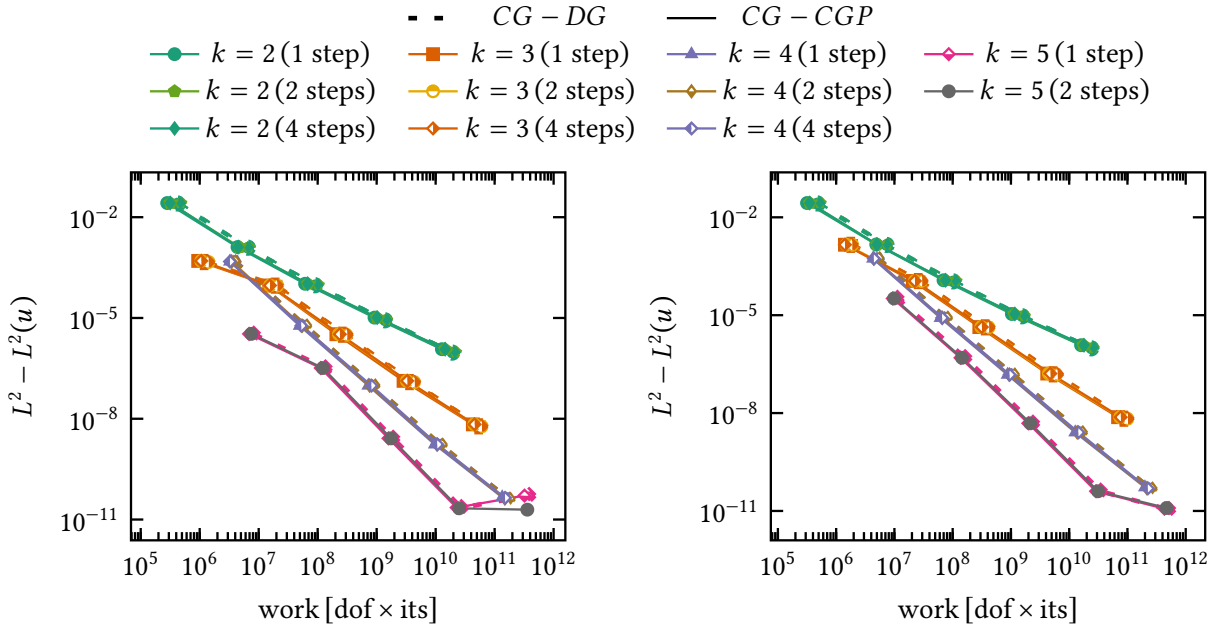
We verify the accuracy of the  $CG(k) - DG(k)$  and  $CG(k) - CGP(k)$  methods for  $p = k$ ,  $k \in \{2, 3, 4, 5\}$ . In Figure 2 we observe that the optimal orders of convergence are achieved for Cartesian and perturbed meshes for  $CG(k) - DG(k)$  discretizations. Therefore, the proposed method is robust and accurate across different mesh configurations.

Table 1 summarizes the average number of GMRES iterations required per time step to solve the resulting linear systems. The data shows the solver's grid independence and a moderate increase of the number of iterations with the order of the discretization. A potential solution to this issue is to consider  $p$ -multigrid, as demonstrated in [25] or by vertex-patch based smoothers [54, 48, 60]. On perturbed meshes, there is a slight increase in the number of GMRES iterations compared to the Cartesian meshes. However, this difference diminishes with further mesh refinement. Collecting multiple time steps in one system does not significantly increase the iteration counts.

To quantify the efficiency and investigate the missing robustness with respect to the polynomial order, Figure 3 presents the accuracy in terms of the  $L^2 - L^2$  error over the work  $w$  defined as:

$$w = \sum_{i=1}^{|\mathcal{T}_\tau|} N^t \times N^x \times N_i^{it} \quad (35)$$

where  $N_i^{it}$  denotes the number of GMRES iterations performed for solving the local subproblem on interval  $I_i$ . Thereby, the work accounts for the computational workload of the global space-time problems. Figure 3 shows that higher order discretizations are more efficient. Despite a moderate increase in the number of iterations, they provide significantly higher accuracy per unit of work. This gain in efficiency, which balances computational effort with accuracy improvements, proves the advantages of higher order discretizations.



**Figure 3:** Calculated  $L^2 - L^2(u)$ -errors of the heat equation for different polynomial orders plotted over the work (35) on Cartesian meshes (left) and perturbed meshes (right). The advantage of higher order discretizations can be observed.

**Table 1:** Table with the number of GMRES iterations until convergence for different polynomial degrees  $k$  and number of refinements  $r$ . We show the numbers for the Cartesian mesh (left) and the perturbed mesh (right) for the  $CG(k) - DG(k)$  discretization of the heat equation.

<b>(a) <math>CG(k) - DG(k)</math> discretizations on a Cartesian mesh (left) and a perturbed mesh (right).</b>											
$k \setminus r$	2	3	4	5	6	$k \setminus r$	2	3	4	5	6
2	9.0	8.75	7.75	6.813	5.938	2	9.0	9.75	9.00	8.875	8.656
3	11.0	9.75	8.88	7.688	6.188	3	12.0	11.75	10.88	10.188	10.563
4	14.0	12.75	10.88	9.500	7.688	4	14.5	14.00	12.88	11.813	11.781
5	16.5	14.25	12.75	10.688	8.568	5	15.0	14.50	13.63	12.563	11.781

<b>(b) <math>CG(k) - CGP(k)</math> discretizations on a Cartesian mesh (left) and a perturbed mesh (right).</b>											
$k \setminus r$	2	3	4	5	6	$k \setminus r$	2	3	4	5	6
2	8	8.75	8.125	7.875	6.938	2	9.0	9.75	9.25	8.875	8.688
3	8	8.75	7.875	6.938	6.563	3	12.0	12.00	10.88	10.188	10.594
4	11	11.25	10.625	9.063	7.938	4	14.5	14.00	12.88	11.875	11.781
5	11	12.00	10.875	9.875	8.781	5	15.0	14.50	13.63	12.563	11.813

<b>(c) <math>CG(k) - DG(k)</math> with 2 time steps at once on a Cartesian mesh (left) and a perturbed mesh (right).</b>											
$k \setminus r$	2	3	4	5	6	$k \setminus r$	2	3	4	5	6
2	9	9	9.00	8.344	7.813	2	10	10.0	10.00	9.60	9.234
3	9	9	8.69	7.875	6.938	3	12	12.38	11.75	10.88	11.484
4	11	12	11.19	9.875	8.813	4	15	15.0	13.75	12.88	12.750

<b>(d) <math>CG(k) - CGP(k)</math> with 2 time steps at once on a Cartesian mesh (left) and a perturbed mesh (right).</b>											
$k \setminus r$	2	3	4	5	6	$k \setminus r$	2	3	4	5	6
2	9.00	9.38	9.00	8.59	7.813	2	10.0	10.00	10.00	9.750	9.484
3	9.00	9.00	8.68	7.88	6.938	3	12.8	13.00	11.75	10.875	11.484
4	11.75	12.38	11.19	9.88	8.813	4	15.0	15.00	13.75	12.875	12.750

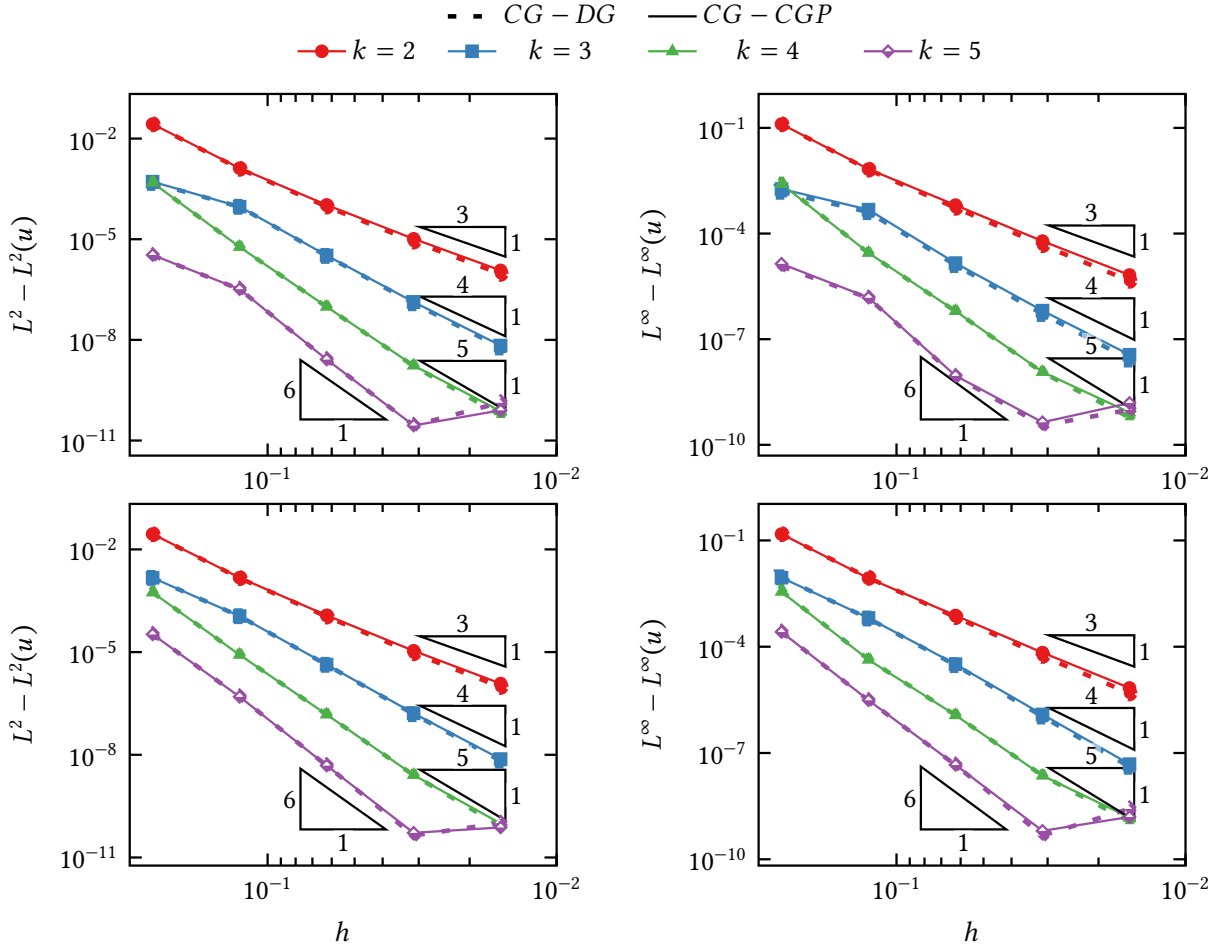
<b>(e) <math>CG(k) - DG(k)</math> with 4 time steps at once on a Cartesian mesh (left) and a perturbed mesh (right).</b>											
$k \setminus r$	2	3	4	5	6	$k \setminus r$	2	3	4	5	6
2	9	9	9.0	8.5	7.75	2	10	10	10	9.75	9.625
3	9	9	9.0	8.0	7.00	3	12	13	12	11.50	11.750
4	11	12	11.5	10.0	9.50	4	15	15	14	13.25	13.125

<b>(f) <math>CG(k) - CGP(k)</math> with 4 time steps at once on a Cartesian mesh (left) and a perturbed mesh (right).</b>											
$k \setminus r$	2	3	4	5	6	$k \setminus r$	2	3	4	5	6
2	9.00	9.00	9.00	8.75	7.88	2	10	10	10	10.0	9.75
3	9.00	9.00	9.00	8.00	7.00	3	12	13	12	11.5	11.75
4	11.00	12.00	12.00	10.00	8.88	4	15	15	14	13.5	13.25



### 4.1.2 Convergence tests of the wave equation



**Figure 4:** Calculated errors for the displacement  $u$  for different orders on Cartesian (top row) and perturbed meshes (bottom row) for  $CG(k) - DG(k)$  (dashed) and  $CG(k) - CGP(k)$  (solid) discretizations of the wave equation. The expected orders of convergence  $k + 1$ , match with the experimental orders.

We perform the convergence tests for the systems (19) and (26). Similar to the heat equation in Section 4.1.1, we test the wave equation on a Cartesian and a perturbed mesh. The perturbed mesh is generated analogously to the one in Section 4.1.1.

We verify the accuracy of the  $CG(k) - DG(k)$  and  $CG(k) - CGP(k)$  methods for  $p = k$ ,  $k \in \{2, 3, 4, 5\}$ . In Figure 4 we observe that the optimal orders of convergence are achieved for Cartesian and perturbed meshes for  $CG(k) - DG(k)$  and  $CG(k) - CGP(k)$  discretizations. The proposed method is robust and accurate across different mesh configurations for the heat and wave equation. The continuous and discontinuous time discretizations lead to similar errors.

Table 2 summarizes the average number of GMRES iterations required per time step to solve the resulting linear systems. Similar to the heat equation, the data shows the solver's grid independence, but we don't achieve full independence of the order of the discretization. On perturbed meshes, there is a slight increase in the number of GMRES iterations compared to the Cartesian meshes. However, this difference vanishes with the mesh refinement. With regard to the iteration counts, the  $CG(k) - CGP(k)$  and  $CG(k) - DG(k)$  discretizations in Table 2 exhibit comparable performance. The solver's performance

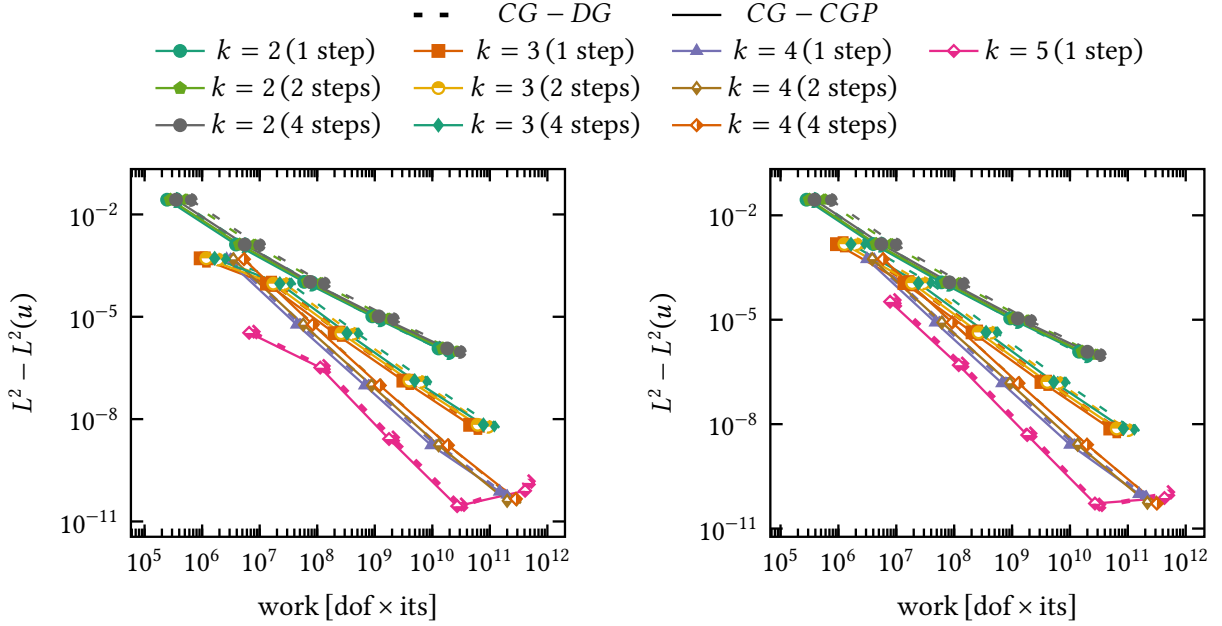


**Figure 5:** Calculated  $L^2 - L^2(u)$ -errors of the wave equation for different orders plotted over the work on Cartesian meshes (left) and perturbed meshes (right). Higher-order discretizations are beneficial.

is similar for the wave and heat equation, except for the fact, that the collection of multiple time steps in one system leads to an increase of the number of GMRES iterations.

To quantify the efficiency and investigate the missing robustness with respect to the polynomial order, Figure 5 presents the accuracy in terms of the  $L^2 - L^2$  error over the work  $w$  as defined in (35). Analogous to the investigations on the heat equation, Figure 5 shows that higher order discretizations are more efficient. Despite a moderate increase in the number of iterations, they provide significantly higher accuracy per unit of work. This gain in efficiency can be observed for the heat and wave equation in the context of the proposed STMG method. In Figure 5 we observe that, in contrast to Figure 3, the amount of work increases with the number of time steps collected in one system. This is of course expected due to the increase of GMRES iterations. Further, Figure 5 illustrates that the continuous discretization method exhibits an advantage over the discontinuous time discretizations. This is due to the smaller number of temporal degrees of freedom resulting from the continuity constraint, as discussed in Section 2.2. Due to the large scales involved, the differences are understated in the plot. To illustrate, consider the case of  $k = 5$  with the largest refinement, resulting in 5 and 6 temporal degrees of freedom per local subproblem on  $I_n$  for the continuous and discontinuous time discretization. Therefore, the number of global degrees of freedom is 36 522 640 000 and 43 827 168 000 for  $CG(k) - CGP(k)$  and  $CG(k) - DG(k)$ . Whether the advantage of having  $\frac{1}{k+1}$  less degrees of freedom for the same level of accuracy materializes in a decreased time to solution depends on the number of iterations (cf. Table 2), the underlying hardware and scaling of the software and on the problem. In the context of dynamic poroelasticity simulations for instance, the authors of [5] observed that continuous time discretizations are efficient, yet not clearly superior to discontinuous methods. In the convergence tests within this section,  $CG(k) - DG(k)$  discretizations exhibited runtimes nearly double those of their continuous counterparts. This unexpected difference will be investigated in the following section by extensive scaling tests. The node configurations and simulation parameters in this section were selected to ensure that the simulations are completed within a specified timeframe and not optimized for optimal performance.

**Table 2:** Tables with the number of GMRES iterations until convergence for different polynomial degrees  $k$  and number of refinements  $r$ . We show the numbers for the Cartesian mesh (left) and the perturbed mesh (right) for the  $CG(k) - DG(k)$  discretization of the wave equation.

<b>(a) <math>CG(k) - DG(k)</math> discretizations on a Cartesian mesh (left) and a perturbed mesh (right).</b>											
$k \setminus r$	2	3	4	5	6	$k \setminus r$	2	3	4	5	6
2	6.5	7.00	7.000	6.938	6.906	2	7.0	7.00	7.000	6.938	6.906
3	8.0	7.75	7.875	7.813	7.563	3	8.5	8.00	8.000	7.938	7.844
4	9.0	9.75	9.875	9.375	8.813	4	10.5	10.75	9.875	9.500	9.156
5	10.5	11.50	11.875	11.563	10.844	5	12.5	12.25	11.875	11.625	11.375

<b>(b) <math>CG(k) - CGP(k)</math> discretizations on a Cartesian mesh (left) and a perturbed mesh (right).</b>											
$k \setminus r$	2	3	4	5	6	$k \setminus r$	2	3	4	5	6
2	7.0	7.75	7.875	7.750	6.969	2	8.0	8.00	8.000	7.938	7.813
3	8.0	7.75	7.625	7.625	6.969	3	8.0	8.00	7.875	7.813	7.625
4	9.0	10.00	9.875	8.938	8.750	4	10.5	10.75	9.875	9.438	9.219
5	10.5	12.00	12.125	11.750	11.219	5	12.5	12.75	12.500	11.750	11.750

<b>(c) <math>CG(k) - DG(k)</math> with 2 time steps at once on a Cartesian mesh (left) and a perturbed mesh (right).</b>											
$k \setminus r$	2	3	4	5	6	$k \setminus r$	2	3	4	5	6
2	10.0	10.88	10.44	10.00	9.73	2	10	10.00	10.00	9.60	9.234
3	12.0	11.88	11.94	11.47	11.73	3	12	12.38	11.75	10.88	11.484
4	14.8	15.88	14.94	14.44	13.77	4	15	15.00	13.75	12.88	12.750

<b>(d) <math>CG(k) - CGP(k)</math> with 2 time steps at once on a Cartesian mesh (left) and a perturbed mesh (right).</b>											
$k \setminus r$	2	3	4	5	6	$k \setminus r$	2	3	4	5	6
2	9.00	9.38	9.00	8.59	7.813	2	10.0	10	10.00	9.750	9.484
3	9.00	9.00	8.68	7.88	6.938	3	12.8	13	11.75	10.875	11.484
4	11.75	12.38	11.19	9.88	8.813	4	15.0	15	13.75	12.875	12.750

<b>(e) <math>CG(k) - DG(k)</math> with 4 time steps at once on a Cartesian mesh (left) and a perturbed mesh (right).</b>											
$k \setminus r$	2	3	4	5	6	$k \setminus r$	2	3	4	5	6
2	12	13	11.5	11.75	10.88	2	14	13	12.5	11.75	11.88
3	16	15	14.5	14.50	13.75	3	18	17	15.5	15.00	14.88
4	20	20	19.0	18.50	18.88	4	22	22	20.0	19.50	19.00

<b>(f) <math>CG(k) - CGP(k)</math> with 4 time steps at once on a Cartesian mesh (left) and a perturbed mesh (right).</b>											
$k \setminus r$	2	3	4	5	6	$k \setminus r$	2	3	4	5	6
2	10	11	10.0	10.0	9.88	2	11	11	11.0	10.75	10.88
3	14	13	12.5	12.0	11.88	3	14	14	13.5	12.75	12.88
4	18	19	18.0	17.5	16.75	4	20	21	19.0	18.50	18.75

## 4.2 Practical example motivated by structural health monitoring

We consider a 3D test problem inspired by [7, Example 5.4]. Let  $\Omega \times I = [-1, 1]^3 \times [0, 2] \subset \mathbb{R}^3 \times \mathbb{R}$  and the initial values be

$$u_0^0(\mathbf{x}) = e^{-|\mathbf{x}s^{-1}|^2} (1 - |\mathbf{x}s^{-1}|^2) \Theta(1 - |\mathbf{x}s^{-1}|), \quad v = 0, \quad (36)$$

where  $\Theta$  is the Heaviside function and  $s = 0.01$ . We choose the speed of sound as

$$\rho = \begin{cases} 1 & \text{for } y < 0.2, \\ 9 & \text{for } y \geq 0.2 \text{ and } z < 0.2, \\ 16 & \text{for } y \geq 0.2 \text{ and } z \geq 0.2. \end{cases} \quad (37)$$

To resolve the coefficients, we utilize a uniform Cartesian mesh consisting of  $5 \times 5 \times 5$  cells as an initial coarse mesh. The problem is relevant to critical applications in structural health monitoring, geophysics, and seismology. The ability to accurately predict the arrival time of signals at specific locations is essential for the analysis of structural integrity and seismic events in these fields. The test problem serves as a foundational model for simulating complex wave propagation. As goal quantities we define point evaluations of the displacement  $u$  at the 3 points  $\mathbf{x}_1 = (0.75, 0, 0)^\top$ ,  $\mathbf{x}_2 = (0, 0, 0.75)^\top$ ,  $\mathbf{x}_3 = (0.75, 0.1, 0.75)^\top$ . The computational tests use up to 256 nodes and all cores of the compute nodes are used.

**Heterogeneous Coefficients** Similar to the numerical convergence tests, the initial time mesh  $\mathcal{T}_\tau$  consists of an  $r + 1$  times uniformly refined interval  $I$ , while the initial spatial mesh  $\mathcal{T}_h$  consists of the  $r$  times uniformly refined hypercube  $\Omega$ . For the strong scaling test shown in Figure 6 we set  $r = 5$ , which results in 320 time cells and 4 096 000 space cells. We were able to obtain a value  $r = 6$  and  $k = 2$ . Higher orders for  $r=6$  were not tested due to a lack of computational resources. The number of spatial, temporal and global degrees of freedom  $\text{dofs}_\Omega$ ,  $\text{dofs}_\tau$ ,  $\text{dofs}_{\text{global}}$ , average number of GMRES iterations  $\bar{n}_{\text{iter}}$  and maximal throughput for this setting are collected in Table 3.

In our study, we test the STMG algorithm with a fixed number of smoothing steps  $n_{\text{smooth}} \in \{1, 2, 4\}$ . The variable  $V$ -cycle proposed in [12] was tested but did not lead to an advantage in terms of iteration count and runtimes. When the variable setting is used, the number of smoothing steps is doubled at each coarser level. When the coarse mesh is too small to have cells present on all processors this lead to significantly decreased parallel efficiency in our experiments.

We evaluate the performance of the STMG method. The key ingredient for a multigrid method is the smoother. The results demonstrate satisfactory performance of the ASM smoother. However, it is important to note that the computational cost is significant due to the use of an inner direct solver, although it is only space-time cell-wise. The cost increases significantly for higher polynomial orders, which presents a challenge for scalability, as the computational costs for the smoother begins to dominate. We observe this in Figure 6, where we plot predictions of the wall times for discretizations of degree  $k$  based on the wall times of the discretizations of degree  $k - 1$  and the computational complexity of the smoother 30. The predictions get increasingly better for more smoothing steps and higher order. Therefore, the runtime and scaling are primarily determined by the smoother. Later, we also substantiate this further for a similar test with larger inhomogeneity. However, the dominance of the smoother attests to the high performance and efficiency of the matrix-free framework. We observe in Figure 6 that the scaling is optimal. For both discretizations, the number of GMRES iterations required for convergence generally increases with higher polynomial degrees  $k$ . Increasing the number of smoothing steps  $n_{\text{smooth}}$  typically reduces the number of GMRES iterations, indicating improved convergence rates. For example, for  $CG(k) - DG(k)$  with  $k = 2$ , the average number of iterations decreases from 13.73 with  $n_{\text{smooth}} = 1$  to 8.78 with  $n_{\text{smooth}} = 2$ . The throughput shows a significant drop with an increase in the number of smoothing steps. The decrease in the number of iterations does not balance the added computational cost per

**Table 3:** Tables with the number of GMRES iterations until convergence for different polynomial degrees  $k$  and number of refinements  $r$ . We show the numbers for the  $CG(k) - DG(k)$  and  $CG(k) - CGP(k)$  discretization of the wave equation. The last entry separated by a rule is a value for  $r = 6$ .

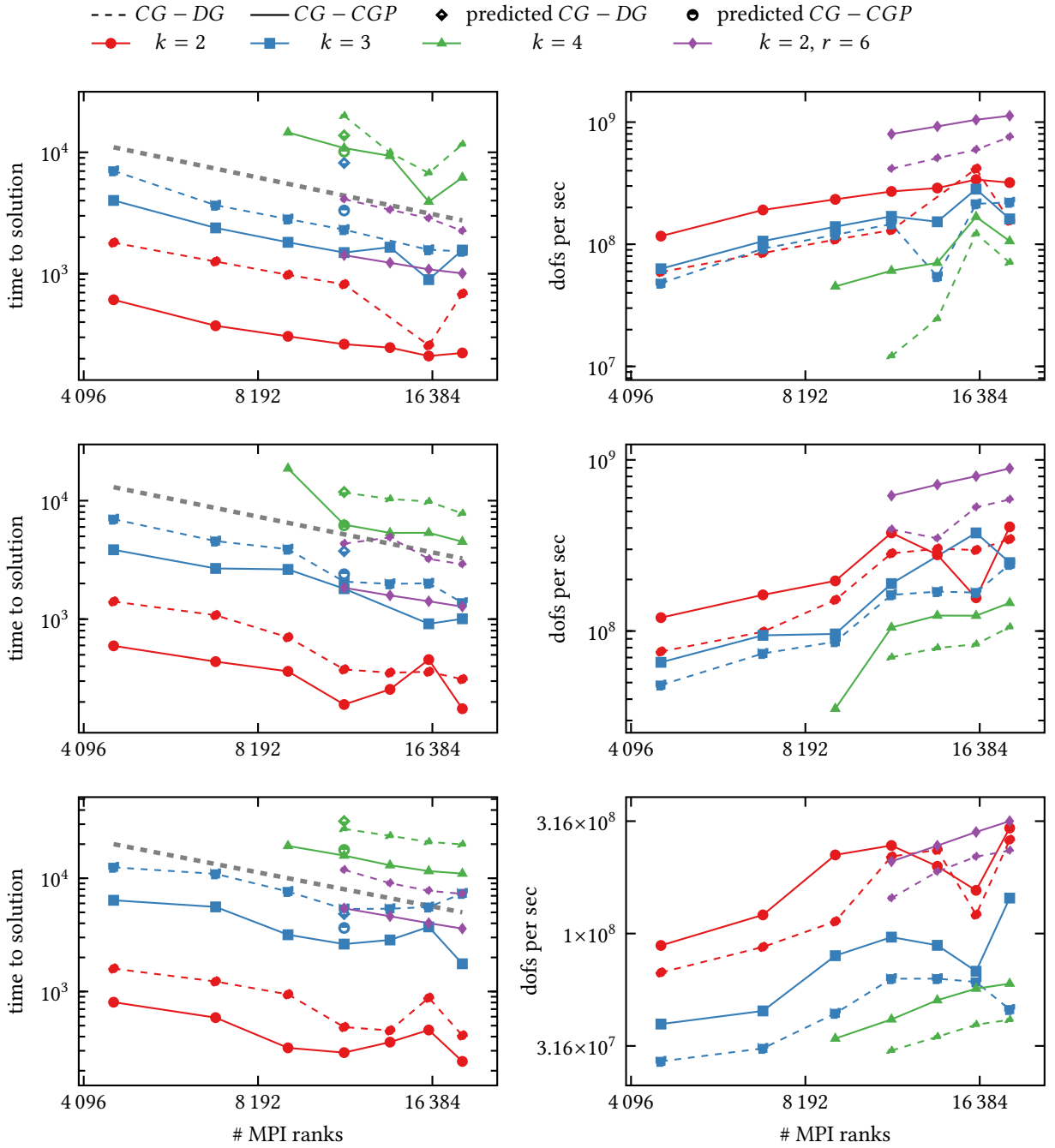
(a) Iterations for $CG(k) - DG(k)$ discretizations with different numbers of smoothing steps ( $n_{\text{smooth}}$ ).										
$k$	dofs $_{\Omega}$	dofs $_{\tau}$	dofs $_{\text{global}}$	$n_{\text{smooth}} = 1$		$n_{\text{smooth}} = 2$		$n_{\text{smooth}} = 4$		
				$\bar{n}_{\text{iter}}$	max dofs/sec	$\bar{n}_{\text{iter}}$	max dofs/sec	$\bar{n}_{\text{iter}}$	max dofs/sec	
2	111 284 641	$3 \times 320$	106 833 255 360	13.73	414 886 429	8.78	343 515 291	5.82	261 014 550	
3	263 374 721	$4 \times 320$	337 119 642 880	13.97	220 339 636	8.81	244 999 740	7.32	62 989 338	
4	513 922 401	$5 \times 320$	822 275 841 600	19.79	121 872 808	12.32	105 419 980	10.34	41 326 994	
2	887 503 681	$3 \times 640$	1 704 007 067 520	12.99	756 328 037	8.87	586 779 293	5.76	234 034 757	

(b) Iterations for $CG(k) - CGP(k)$ discretizations with different numbers of smoothing steps.										
$k$	dofs $_{\Omega}$	dofs $_{\tau}$	dofs $_{\text{global}}$	$n_{\text{smooth}} = 1$		$n_{\text{smooth}} = 2$		$n_{\text{smooth}} = 4$		
				$\bar{n}_{\text{iter}}$	max dofs/sec	$\bar{n}_{\text{iter}}$	max dofs/sec	$\bar{n}_{\text{iter}}$	max dofs/sec	
2	111 284 641	$2 \times 320$	71 222 170 240	11.51	338 508 413	7.83	406 055 703	5.46	294 671 784	
3	263 374 721	$3 \times 320$	252 839 732 160	11.06	282 565 637	6.88	251 082 157	5.77	143 822 373	
4	513 922 401	$4 \times 320$	657 820 673 280	16.25	167 640 334	10.13	146 020 127	8.16	59 856 294	
2	887 503 681	$2 \times 640$	1 136 004 711 680	11.19	1 126 988 801	7.82	890 984 088	5.62	316 259 664	

iteration. Higher polynomial degrees result in lower throughput due to the increased complexity of the smoother. The  $CG(k) - DG(k)$  discretization generally requires more GMRES iterations compared to the  $CG(k) - CGP(k)$  discretization for the same polynomial degree and smoothing steps. The throughput for  $CG(k) - CGP(k)$  discretizations is consistently higher than for  $CG(k) - DG(k)$  discretizations, suggesting better efficiency of the continuous time discretization. At the same time, considering the point evaluations plotted in Figure 7, we see that the  $CG(k) - DG(k)$  discretization shows better convergence behavior compared to the  $CG(k) - CGP(k)$  approach, due to the inhomogeneous material. As evidenced by the same figure, both discretizations converge to the same solution. As the resolution of the heterogeneities improves, the benefit of discontinuous discretization becomes less pronounced. The advantage of higher-order discretizations persists. The  $k = 2, r = 6$  case achieves the highest throughputs, with wall clock times that are slightly higher than those with  $k = 3, r = 5$  (cf. Figure 6). However, Figure 7 shows that the  $k = 3, r = 5$  discretization performs at least as well as the  $k = 2, r = 6$  one.

The high cost of the smoother represents a limitation in terms of the throughput in degrees of freedom per second. In the convergence tests, higher order discretizations demonstrated superior accuracy per work, while they now seem to be disadvantageous in terms of the time to solution. We stress that this is solely due to the increasingly expensive smoother. Therefore, future work should focus on developing more efficient smoothers. A straightforward improvement could be replacing the inner direct solver. Despite the high costs of the smoother, it is quite robust as indicated by the consistent iteration counts observed in all the performed tests. We note that the appeal of the proposed space-time smoother is its wide applicability in fluid mechanics [1, 3], solid mechanics [68], fluid-structure interaction [22] and dynamic poroelasticity [4]. This robustness together with the excellent scalability will enable the efficient solution of large-scale coupled problems in future work.



**Figure 6:** Strong scaling test results for the STMG algorithm with varying numbers of smoothing steps. Each row corresponds to a different number of smoothing steps: 1, 2, and 4 from top to bottom. The left column shows the time to solution as a function of the number of MPI processes. The dashed gray lines indicate the optimal scaling. The half-squares and half-circles indicate the predicted runtime of the  $CG(k)$ - $DG(k)$  and  $CG(k)$ - $CGP(k)$  discretization, based on the wallclock time of one degree lower and (30). The right column depicts the degrees of freedom (dofs) processed per second over the number of MPI processes.

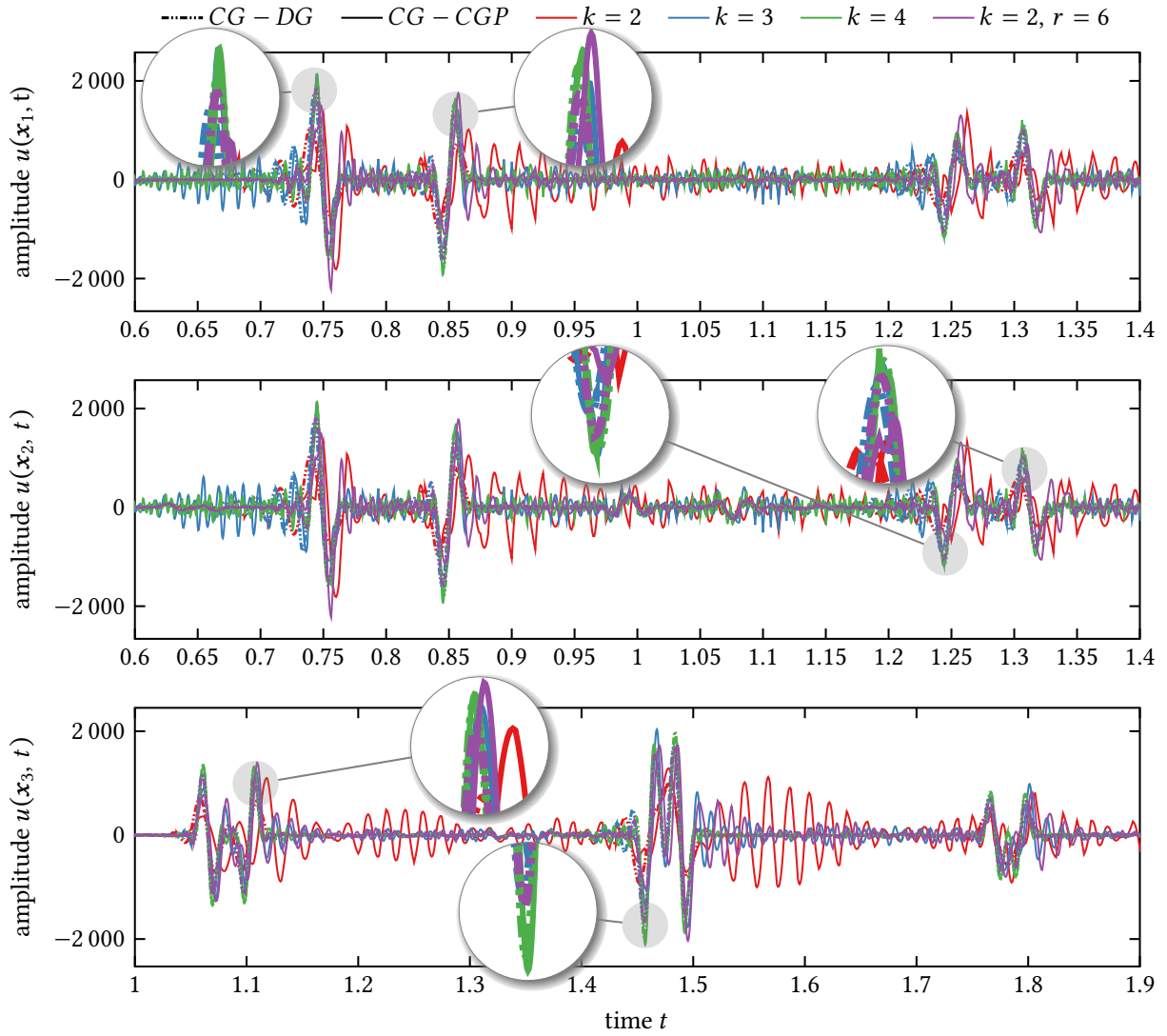


**Figure 7:** Plots of the point evaluations of the displacement at  $x_1$ ,  $x_2$ ,  $x_3$  plotted over subintervals of the time interval  $[0, 2]$ . They are adapted such that the first signal arriving at the point is plotted.

**Highly Heterogeneous Coefficients** To increase the physical realism of our simulations, we incorporate highly heterogeneous materials with rough coefficients and assess the method’s ability to effectively handle discontinuities and complex physical phenomena. To this end, we perturb the coefficient function (37) by sampling  $c \in [0.4, 1.6]$  from a uniform random distribution for each coarse mesh cell and using  $c \cdot \rho$  as the new coefficient. For the numerical examples we use the same settings as for the heterogeneous coefficients. In Figure 9 we show the results of a scaling test analogous to the one in Figure 6. The number of degrees of freedom, number of GMRES iterations and maximal throughput for this setting are collected in Table 4. Analogous to the previous test, we observe in Figure 8 that both discretizations converge to the same solution. In Figure 10 we present the relative timings of different sections of the program during a strong scaling test with a single smoothing step  $n_{\text{smooth}} = 1$ . Each bar represents a different run, and the segments of the bar indicate the proportion of total execution time spent in various components of the program. The “GMG w/o Smoother” section represents the time spent in the STMG method, excluding the smoothing steps, i. e. only operator evaluations and transfers. The proportion of this component remains almost constant as the number of nodes increases. The “Smoother” section shows the time spent in the ASM smoother. This is the computationally most intensive part of the program, and the polynomial order has a significant impact on the time. The proportion decreases slightly with an increasing number of nodes, but it is always the dominant factor in wall clock time. The “Operator w/o GMG” section shows the time spent in the operator, excluding the ones in the STMG preconditioner. For lower order discretizations, this part becomes more significant with an increasing number of nodes due to the communication in combination with the low arithmetic intensity. The “Other” section represents the remaining time not accounted for by the other components, i. e. the assembly of source terms, evaluation of goal quantities, and operations performed in between time steps. For lower order discretizations, this part also increases with an increasing number of nodes due to the communication.

**Table 4:** Tables with the number of GMRES iterations until convergence for different polynomial degrees  $k$  and number of refinements  $r$ . We show the numbers for the  $CG(k) - DG(k)$  and  $CG(k) - CGP(k)$  discretization of the wave equation. The last entry separated by a rule is a value for  $r = 6$ .

(a) Iterations for $CG(k) - DG(k)$ discretizations with different numbers of smoothing steps ( $n_{\text{smooth}}$ ).										
$k$	dofs $_{\Omega}$	dofs $_{\tau}$	dofs $_{\text{global}}$	$n_{\text{smooth}} = 1$		$n_{\text{smooth}} = 2$		$n_{\text{smooth}} = 4$		
				$\bar{n}_{\text{iter}}$	max dofs/sec	$\bar{n}_{\text{iter}}$	max dofs/sec	$\bar{n}_{\text{iter}}$	max dofs/sec	
2	111 284 641	$3 \times 320$	106 833 255 360	12.75	386 656 733	9.55	324 031 712	6.59	212 392 158	
3	263 374 721	$4 \times 320$	337 119 642 880	12.83	294 170 718	9.50	228 555 690	7.38	106 548 560	
4	513 922 401	$5 \times 320$	822 275 841 600	17.96	128 380 303	13.51	96 341 633	10.94	47 862 389	
2	887 503 681	$3 \times 640$	1 704 007 067 520	14.25	691 000 432	9.48	553 608 534	6.54	199 977 358	
(b) Iterations for $CG(k) - CGP(k)$ discretizations with different numbers of smoothing steps.										
$k$	dofs $_{\Omega}$	dofs $_{\tau}$	dofs $_{\text{global}}$	$n_{\text{smooth}} = 1$		$n_{\text{smooth}} = 2$		$n_{\text{smooth}} = 4$		
				$\bar{n}_{\text{iter}}$	max dofs/sec	$\bar{n}_{\text{iter}}$	max dofs/sec	$\bar{n}_{\text{iter}}$	max dofs/sec	
2	111 284 641	$2 \times 320$	71 222 170 240	10.91	488 827 524	7.75	409 322 817	5.63	276 805 947	
3	263 374 721	$3 \times 320$	252 839 732 160	10.83	455 567 085	7.66	352 291 671	5.64	128 999 863	
4	513 922 401	$4 \times 320$	657 820 673 280	15.06	251 168 624	10.70	149 165 685	8.34	64 366 015	
2	887 503 681	$2 \times 640$	1 136 004 711 680	11.65	886 119 119	7.80	877 901 632	5.66	278 227 948	

The results of the tests for a problem with higher heterogeneity are summarized in Table 4. The tests include  $CG(k) - DG(k)$  and  $CG(k) - CGP(k)$  discretizations. Similar to our previous findings, we observe



that the number of GMRES iterations required for convergence increases with higher polynomial degrees  $k$ . Increasing the number of smoothing steps  $n_{\text{smooth}}$  reduces the number of GMRES iterations. For example, for  $CG(k) - DG(k)$  with  $k = 2$ , the average number of iterations decreases from 12.75 with  $n_{\text{smooth}} = 1$  to 9.55 with  $n_{\text{smooth}} = 2$ . Again, the  $CG(k) - DG(k)$  discretization generally requires more GMRES iterations compared to the  $CG(k) - CGP(k)$  discretization for the same polynomial degree and smoothing steps. The throughput for  $CG(k) - CGP(k)$  discretizations is consistently higher than for  $CG(k) - DG(k)$  discretizations.

While more smoothing steps improve convergence by reducing the iteration count, less smoothing steps are again beneficial in terms of the time to solution. Overall, the results with larger inhomogeneity are consistent with our previous findings. The larger inhomogeneity does not substantially change the convergence and scalability of the method.

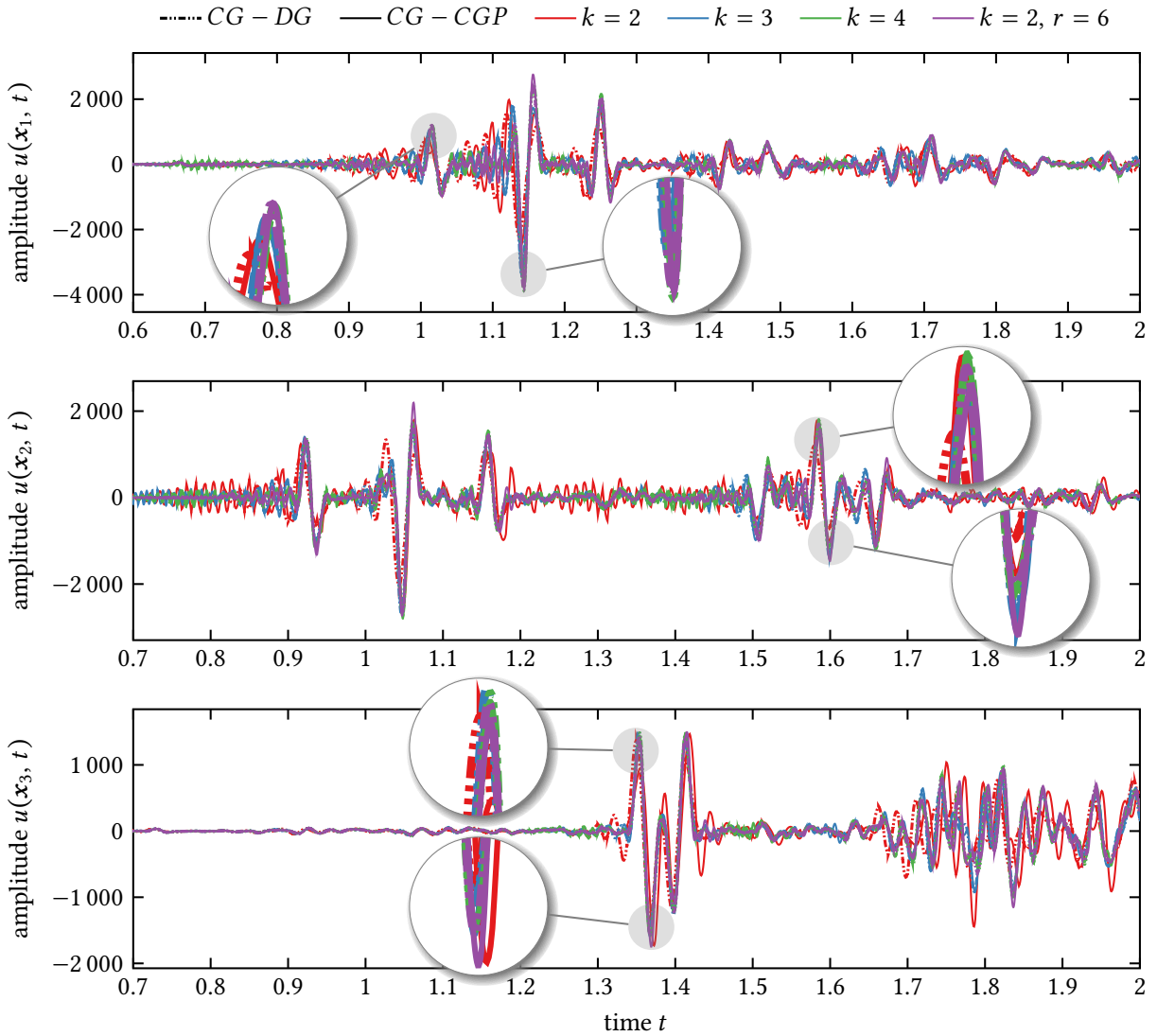


**Figure 8:** Plots of the point evaluations of the displacement at  $x_1$ ,  $x_2$ ,  $x_3$  plotted over subintervals of the time interval  $[0, 2]$ . They are adapted such that the first signal arriving at the point is plotted.

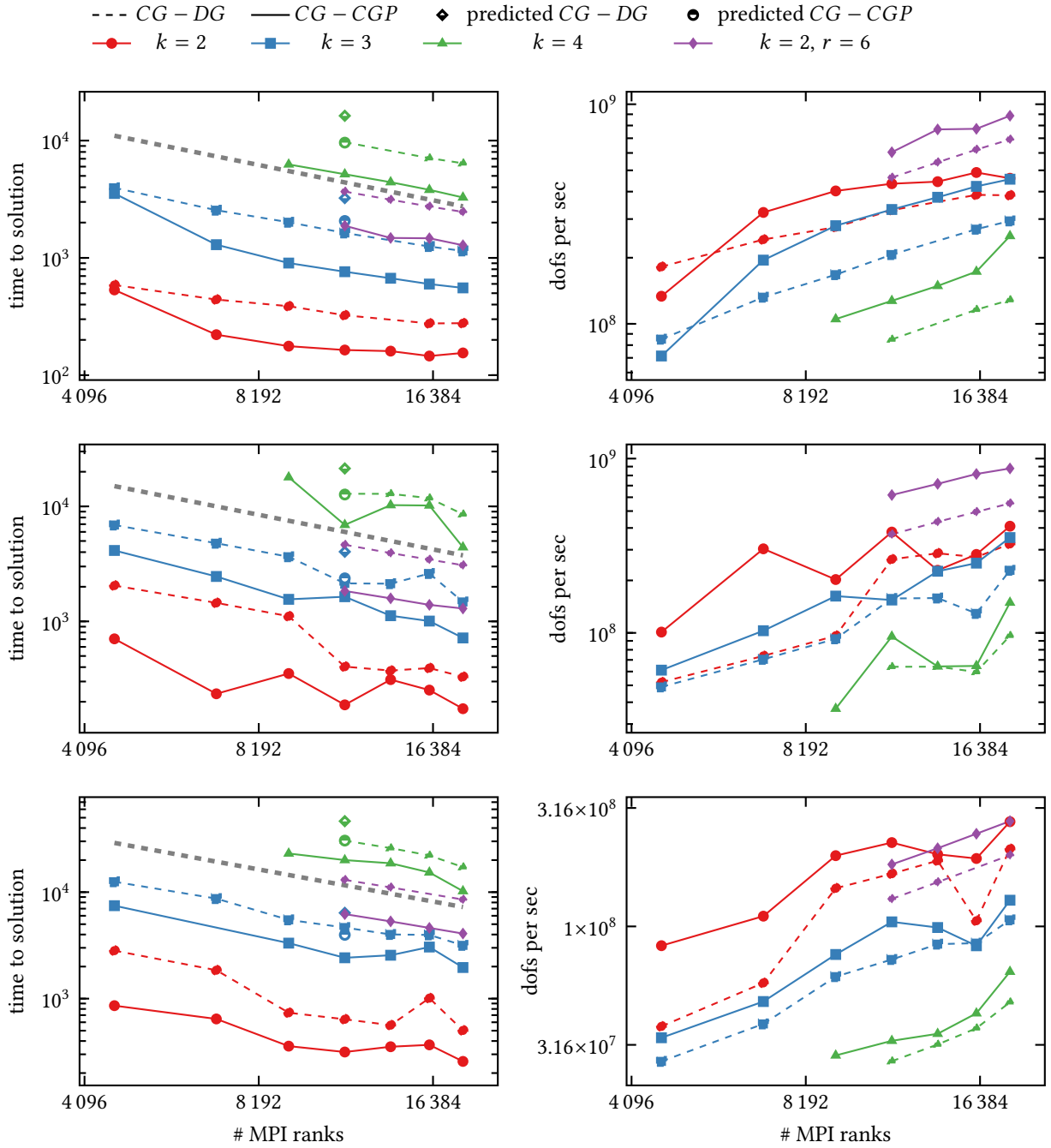


**Figure 9:** Strong scaling test results for the STMG algorithm with varying numbers of smoothing steps. Each row corresponds to a different number of smoothing steps: 1, 2, and 4 from top to bottom. The left column shows the time to solution as a function of the number of MPI processes. The dashed gray lines indicate the optimal speedup. The half-squares and half-circles indicate the predicted runtime of the  $CG(k)$ - $DG(k)$  and  $CG(k)$ - $CGP(k)$  discretization, based on the wallclock time of one degree lower and (30). The right column depicts the degrees of freedom (dofs) processed per second over the number of MPI processes.

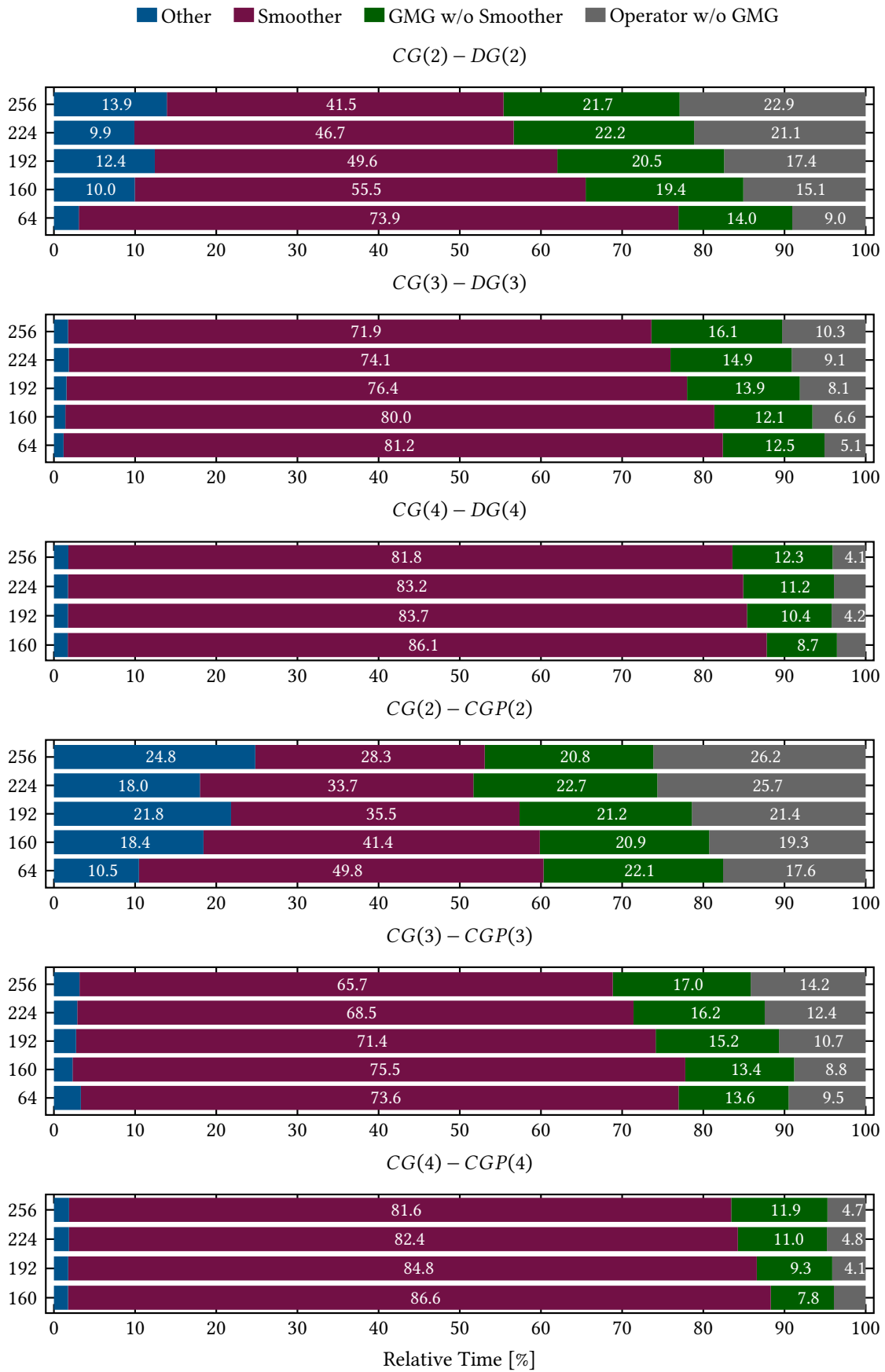


Figure 10: Time spent on different sections of the program in the strong scaling tests.

## 5 Conclusion

We verified the accuracy and robustness of the  $CG(p) - DG(k)$  and  $CG(p) - CGP(k)$  methods for various polynomial orders on both Cartesian and perturbed meshes. The proposed STMG method achieved optimal convergence and grid independence. While we were not able to achieve independence of the polynomial order, the increase with the number of iterations was moderate. We note that robustness w. r. t. the polynomial order can be obtained by vertex-patch based smoothers [54, 48, 60] or  $p$ -multigrid [25], which is a straightforward extension to the space-time cell wise ASM smoother. However, the critical bottleneck for higher polynomial orders is the computationally expensive smoother. Thus, the inner direct solver should be replaced by a more computationally less expensive alternative before turning to patch based smoothers. In light of the preceding remarks, it is important to emphasize that the method demonstrates remarkable performance. It achieves throughputs of over a billion degrees of freedom per second on problems with more than a trillion degrees of freedom and exhibits optimal scaling in our tests. Notably, it outperforms existing matrix-based implementations by orders of magnitude.

We observed that, while an increase of the number of smoothing steps improves convergence rates, it also has a negative impact on the throughput due to higher computational costs. The reduction of GMRES iterations does not result in a reduction of the time to solution, as the increased number of smoothing steps counteract this effect. The  $CG(p) - CGP(k)$  discretization shows better efficiency compared to  $CG(p) - DG(k)$ . These advantages cannot be conclusively verified in the context of problems with discontinuous material coefficients. To investigate this further, we will examine the problems with discontinuous material coefficients presented here with  $DG(p) - DG(k)$  discretizations and first-order formulations in space and time.

Higher-order discretizations achieve greater accuracy compared to lower-order ones, owing to their efficiency in using fewer resources to attain the same level of precision. In the convergence tests, we verified this in terms of the accuracy per work. In the scaling tests, higher-order discretizations appeared to be less advantageous in terms of time to solution. We established that the high cost of the smoother is the reason for this. Despite its high cost, the smoother exhibited excellent performance across multiple applications. Overall, the proposed matrix-free space-time finite element method within a space-time multigrid framework is efficient and scalable, making it a promising candidate for large-scale problems in fluid mechanics, fluid-structure interaction, and dynamic poroelasticity.

## Acknowledgement

Computational resources (HPC cluster HSUper) have been provided by the project hpc.bw, funded by dtec.bw - Digitalization and Technology Research Center of the Bundeswehr. dtec.bw is funded by the European Union - NextGenerationEU.

## References

- [1] N. Ahmed et al. “An Assessment of Some Solvers for Saddle Point Problems Emerging from the Incompressible Navier–Stokes Equations”. In: *Computer Methods in Applied Mechanics and Engineering* 331 (Apr. 1, 2018), pp. 492–513. ISSN: 0045-7825. DOI: [10.1016/j.cma.2017.12.004](https://doi.org/10.1016/j.cma.2017.12.004).
- [2] J. Angel, S. Götschel, and D. Ruprecht. *Impact of Spatial Coarsening on Parareal Convergence*. Version 1. Nov. 19, 2021. DOI: [10.48550/arXiv.2111.10228](https://doi.org/10.48550/arXiv.2111.10228). preprint.
- [3] M. Anselmann and M. Bause. “A Geometric Multigrid Method for Space-Time Finite Element Discretizations of the Navier–Stokes Equations and Its Application to 3d Flow Simulation”. In: *ACM Transactions on Mathematical Software* (Feb. 1, 2023). ISSN: 0098-3500. DOI: [10.1145/3582492](https://doi.org/10.1145/3582492).

- [4] M. Anselmann et al. “An Energy-Efficient GMRES–Multigrid Solver for Space-Time Finite Element Computation of Dynamic Poroelasticity”. In: *Computational Mechanics* (Apr. 13, 2024). ISSN: 1432-0924. DOI: [10.1007/s00466-024-02460-w](https://doi.org/10.1007/s00466-024-02460-w).
- [5] M. Anselmann et al. “Benchmark Computations of Dynamic Poroelasticity”. In: *PAMM* 23.2 (2023), e202300096. ISSN: 1617-7061. DOI: [10.1002/pamm.202300096](https://doi.org/10.1002/pamm.202300096).
- [6] D. Arndt et al. “The Deal.II Library, Version 9.5”. In: *Journal of Numerical Mathematics* 31.3 (Sept. 1, 2023), pp. 231–246. ISSN: 1569-3953. DOI: [10.1515/jnma-2023-0089](https://doi.org/10.1515/jnma-2023-0089).
- [7] W. Bangerth, M. Geiger, and R. Rannacher. “Adaptive Galerkin Finite Element Methods for the Wave Equation”. In: *Comp. Meth. Appl. Math.* 10 (2010), pp. 3–48. DOI: [10.2478/cmam-2010-0001](https://doi.org/10.2478/cmam-2010-0001).
- [8] L. Banjai, E. H. Georgoulis, and O. Lijoka. “A Trefftz Polynomial Space-Time Discontinuous Galerkin Method for the Second Order Wave Equation”. In: *SIAM Journal on Numerical Analysis* 55.1 (Jan. 2017), pp. 63–86. ISSN: 0036-1429. DOI: [10.1137/16M1065744](https://doi.org/10.1137/16M1065744).
- [9] M. Bause, M. P. Bruchhäuser, and U. Köcher. “Flexible Goal-Oriented Adaptivity for Higher-Order Space-Time Discretizations of Transport Problems with Coupled Flow”. In: *Computers & Mathematics with Applications* 91 (June 2021), pp. 17–35. ISSN: 08981221. DOI: [10.1016/j.camwa.2020.08.028](https://doi.org/10.1016/j.camwa.2020.08.028).
- [10] A. Borzi and R. Griesse. “Experiences with a Space–Time Multigrid Method for the Optimal Control of a Chemical Turbulence Model”. In: *International Journal for Numerical Methods in Fluids* 47.8-9 (2005), pp. 879–885. ISSN: 1097-0363. DOI: [10.1002/flid.904](https://doi.org/10.1002/flid.904).
- [11] J. H. Bramble. *Multigrid Methods*. Longman Scientific & Technical, Harlow, 1993. 161 pp.
- [12] J. H. Bramble and J. E. Pasciak. “New Convergence Estimates for Multigrid Algorithms”. In: *Mathematics of Computation* 49.180 (1987), pp. 311–329. ISSN: 0025-5718, 1088-6842. DOI: [10.1090/S0025-5718-1987-0906174-X](https://doi.org/10.1090/S0025-5718-1987-0906174-X).
- [13] B. Chaudet-Dumas, M. J. Gander, and A. Pogozelskyte. *An Optimized Space-Time Multigrid Algorithm for Parabolic PDEs*. Feb. 27, 2023. DOI: [10.48550/arXiv.2302.13881](https://doi.org/10.48550/arXiv.2302.13881). preprint.
- [14] A. J. Christlieb, C. B. Macdonald, and B. W. Ong. “Parallel High-Order Integrators”. In: *SIAM Journal on Scientific Computing* 32.2 (Jan. 2010), pp. 818–835. ISSN: 1064-8275. DOI: [10.1137/09075740X](https://doi.org/10.1137/09075740X).
- [15] F. Danieli and A. J. Wathen. “All-at-Once Solution of Linear Wave Equations”. In: *Numerical Linear Algebra with Applications* 28.6 (2021), e2386. ISSN: 1099-1506. DOI: [10.1002/nla.2386](https://doi.org/10.1002/nla.2386).
- [16] H. De Sterck et al. “Convergence Analysis for Parallel-in-Time Solution of Hyperbolic Systems”. In: *Numerical Linear Algebra with Applications* 27.1 (2020), e2271. ISSN: 1099-1506. DOI: [10.1002/nla.2271](https://doi.org/10.1002/nla.2271).
- [17] M. Donatelli et al. “All-at-Once Multigrid Approaches for One-Dimensional Space-Fractional Diffusion Equations”. In: *Calcolo* 58.4 (Oct. 7, 2021), p. 45. ISSN: 1126-5434. DOI: [10.1007/s10092-021-00436-3](https://doi.org/10.1007/s10092-021-00436-3).
- [18] W. Dörfler, S. Findeisen, and C. Wieners. “Space-Time Discontinuous Galerkin Discretizations for Linear First-Order Hyperbolic Evolution Systems”. In: *Computational Methods in Applied Mathematics* 16.3 (July 1, 2016), pp. 409–428. ISSN: 1609-9389. DOI: [10.1515/cmam-2016-0015](https://doi.org/10.1515/cmam-2016-0015).
- [19] W. Dörfler et al. “2. Parallel Adaptive Discontinuous Galerkin Discretizations in Space and Time for Linear Elastic and Acoustic Waves”. In: *2. Parallel Adaptive Discontinuous Galerkin Discretizations in Space and Time for Linear Elastic and Acoustic Waves*. De Gruyter, Sept. 23, 2019, pp. 61–88. ISBN: 978-3-11-054848-8. DOI: [10.1515/9783110548488-002](https://doi.org/10.1515/9783110548488-002).

- [20] J. Dünnebacke et al. “Increased Space-Parallelism via Time-Simultaneous Newton-multigrid Methods for Nonstationary Nonlinear PDE Problems”. In: *The International Journal of High Performance Computing Applications* 35.3 (May 2021), pp. 211–225. ISSN: 1094-3420, 1741-2846. DOI: [10.1177/10943420211001940](https://doi.org/10.1177/10943420211001940).
- [21] J. Ernesti and C. Wieners. “Space-Time Discontinuous Petrov–Galerkin Methods for Linear Wave Equations in Heterogeneous Media”. In: *Computational Methods in Applied Mathematics* 19.3 (July 1, 2019), pp. 465–481. ISSN: 1609-9389. DOI: [10.1515/cmam-2018-0190](https://doi.org/10.1515/cmam-2018-0190).
- [22] L. Failer and T. Richter. “A Parallel Newton Multigrid Framework for Monolithic Fluid-Structure Interactions”. In: *Journal of Scientific Computing* 82.28 (2021). DOI: [10.1007/s10915-019-01113-y](https://doi.org/10.1007/s10915-019-01113-y).
- [23] R. D. Falgout et al. “Multigrid Methods with Space–Time Concurrency”. In: *Computing and Visualization in Science* 18.4 (Aug. 1, 2017), pp. 123–143. ISSN: 1433-0369. DOI: [10.1007/s00791-017-0283-9](https://doi.org/10.1007/s00791-017-0283-9).
- [24] R. Falgout et al. “Parallel Time Integration with Multigrid”. In: *SIAM Journal on Scientific Computing* 36 (Dec. 18, 2014), pp. C635–C661. DOI: [10.1137/130944230](https://doi.org/10.1137/130944230).
- [25] N. Fehn et al. “Hybrid Multigrid Methods for High-Order Discontinuous Galerkin Discretizations”. In: *Journal of Computational Physics* 415 (Aug. 15, 2020), p. 109538. ISSN: 0021-9991. DOI: [10.1016/j.jcp.2020.109538](https://doi.org/10.1016/j.jcp.2020.109538).
- [26] H. Fischer et al. “MORE DWR: Space-time Goal-Oriented Error Control for Incremental POD-based ROM for Time-Averaged Goal Functionals”. In: *Journal of Computational Physics* 504 (May 1, 2024), p. 112863. ISSN: 0021-9991. DOI: [10.1016/j.jcp.2024.112863](https://doi.org/10.1016/j.jcp.2024.112863).
- [27] S. R. Franco et al. “Multigrid Method Based on a Space-Time Approach with Standard Coarsening for Parabolic Problems”. In: *Applied Mathematics and Computation* 317 (Jan. 15, 2018), pp. 25–34. ISSN: 0096-3003. DOI: [10.1016/j.amc.2017.08.043](https://doi.org/10.1016/j.amc.2017.08.043).
- [28] M. J. Gander. “50 Years of Time Parallel Time Integration”. In: *Multiple Shooting and Time Domain Decomposition Methods*. Ed. by T. Carraro et al. Contributions in Mathematical and Computational Sciences. Cham: Springer International Publishing, 2015, pp. 69–113. ISBN: 978-3-319-23321-5. DOI: [10.1007/978-3-319-23321-5\\_3](https://doi.org/10.1007/978-3-319-23321-5_3).
- [29] M. J. Gander, F. Kwok, and H. Zhang. “Multigrid Interpretations of the Parareal Algorithm Leading to an Overlapping Variant and MGRIT”. In: *Computing and Visualization in Science* 19.3 (July 1, 2018), pp. 59–74. ISSN: 1433-0369. DOI: [10.1007/s00791-018-0297-y](https://doi.org/10.1007/s00791-018-0297-y).
- [30] M. J. Gander and M. Neumüller. “Analysis of a New Space-Time Parallel Multigrid Algorithm for Parabolic Problems”. In: *SIAM Journal on Scientific Computing* 38.4 (Jan. 2016), A2173–A2208. ISSN: 1064-8275, 1095-7197. DOI: [10.1137/15M1046605](https://doi.org/10.1137/15M1046605).
- [31] A. Goddard and A. Wathen. “A Note on Parallel Preconditioning for All-at-Once Evolutionary PDEs”. In: *ETNA - Electronic Transactions on Numerical Analysis* 51 (2019), pp. 135–150. ISSN: 1068-9613, 1068-9613. DOI: [10.1553/etna\\_vol51s135](https://doi.org/10.1553/etna_vol51s135).
- [32] J. Gopalakrishnan, J. Schöberl, and C. Wintersteiger. “Mapped Tent Pitching Schemes for Hyperbolic Systems”. In: *SIAM Journal on Scientific Computing* 39.6 (Jan. 2017), B1043–B1063. ISSN: 1064-8275. DOI: [10.1137/16M1101374](https://doi.org/10.1137/16M1101374).
- [33] W. Hackbusch. *Multi-Grid Methods and Applications*. Springer, 1985.
- [34] W. Hackbusch. “Parabolic Multi-Grid Methods”. In: *Proc. of the Sixth Int’l. Symposium on Computing Methods in Applied Sciences and Engineering, VI*. NLD: North-Holland Publishing Co., June 1, 1985, pp. 189–197. ISBN: 978-0-444-87597-6.

- [35] J. Hahne, B. S. Southworth, and S. Friedhoff. “Asynchronous Truncated Multigrid-Reduction-in-Time”. In: *SIAM Journal on Scientific Computing* 45.3 (June 30, 2023), S281–S306. ISSN: 1064-8275. DOI: [10.1137/21M1433149](https://doi.org/10.1137/21M1433149).
- [36] E. Hairer and G. Wanner. *Solving Ordinary Differential Equations II. Stiff and Differential-Algebraic Problems*. Vol. 14. Computational Mathematics. Springer, 1996.
- [37] C. Hofer et al. “Parallel and Robust Preconditioning for Space-Time Isogeometric Analysis of Parabolic Evolution Problems”. In: *SIAM Journal on Scientific Computing* 41.3 (Jan. 2019), A1793–A1821. ISSN: 1064-8275. DOI: [10.1137/18M1208794](https://doi.org/10.1137/18M1208794).
- [38] S. Hon and S. Serra-Capizzano. “A Block Toeplitz Preconditioner for All-at-Once Systems from Linear Wave Equations”. In: *ETNA - Electronic Transactions on Numerical Analysis* 58 (2023), pp. 177–195. ISSN: 1068-9613, 1068-9613. DOI: [10.1553/etna\\_vol58s177](https://doi.org/10.1553/etna_vol58s177).
- [39] G. Horton and S. Vandewalle. “A Space-Time Multigrid Method for Parabolic Partial Differential Equations”. In: *SIAM Journal on Scientific Computing* 16.4 (July 1995), pp. 848–864. ISSN: 1064-8275. DOI: [10.1137/0916050](https://doi.org/10.1137/0916050).
- [40] U. Köcher and M. Bause. “Variational Space–Time Methods for the Wave Equation”. In: *Journal of Scientific Computing* 61.2 (Nov. 2014), pp. 424–453. ISSN: 0885-7474, 1573-7691. DOI: [10.1007/s10915-014-9831-3](https://doi.org/10.1007/s10915-014-9831-3).
- [41] M. Kronbichler and K. Kormann. “A Generic Interface for Parallel Cell-Based Finite Element Operator Application”. In: *Computers & Fluids* 63 (June 30, 2012), pp. 135–147. ISSN: 0045-7930. DOI: [10.1016/j.compfluid.2012.04.012](https://doi.org/10.1016/j.compfluid.2012.04.012).
- [42] U. Langer and A. Schafelner. “Adaptive Space–Time Finite Element Methods for Parabolic Optimal Control Problems”. In: *Journal of Numerical Mathematics* 30.4 (Dec. 1, 2022), pp. 247–266. ISSN: 1569-3953. DOI: [10.1515/jnma-2021-0059](https://doi.org/10.1515/jnma-2021-0059).
- [43] U. Langer and A. Schafelner. “Space-Time Finite Element Methods for Parabolic Initial-Boundary Value Problems with Non-smooth Solutions”. In: *Large-Scale Scientific Computing*. Ed. by I. Lirkov and S. Margenov. Lecture Notes in Computer Science. Cham: Springer International Publishing, 2020, pp. 593–600. ISBN: 978-3-030-41032-2. DOI: [10.1007/978-3-030-41032-2\\_68](https://doi.org/10.1007/978-3-030-41032-2_68).
- [44] U. Langer and A. Schafelner. “Space-Time Hexahedral Finite Element Methods for Parabolic Evolution Problems”. In: *Domain Decomposition Methods in Science and Engineering XXVI*. Ed. by S. C. Brenner et al. Lecture Notes in Computational Science and Engineering. Cham: Springer International Publishing, 2022, pp. 515–522. ISBN: 978-3-030-95025-5. DOI: [10.1007/978-3-030-95025-5\\_55](https://doi.org/10.1007/978-3-030-95025-5_55).
- [45] U. Langer and O. Steinbach, eds. *Space-Time Methods: Applications to Partial Differential Equations*. De Gruyter, Sept. 23, 2019. ISBN: 978-3-11-054848-8. DOI: [10.1515/9783110548488](https://doi.org/10.1515/9783110548488).
- [46] G. Matthies and F. Schieweck. “Higher Order Variational Time Discretizations for Nonlinear Systems of Ordinary Differential Equations”. In: *Preprint* (2011), p. 30.
- [47] E. McDonald, J. Pestana, and A. Wathen. “Preconditioning and Iterative Solution of All-at-Once Systems for Evolutionary Partial Differential Equations”. In: *SIAM Journal on Scientific Computing* 40.2 (Jan. 2018), A1012–A1033. ISSN: 1064-8275. DOI: [10.1137/16M1062016](https://doi.org/10.1137/16M1062016).
- [48] A. Miraçi, J. Papež, and M. Vohralík. “A Multilevel Algebraic Error Estimator and the Corresponding Iterative Solver with  $\mathbb{P}$ -Robust Behavior”. In: *SIAM Journal on Numerical Analysis* 58.5 (Jan. 2020), pp. 2856–2884. ISSN: 0036-1429. DOI: [10.1137/19M1275929](https://doi.org/10.1137/19M1275929).

- [49] P. Munch and M. Kronbichler. “Cache-Optimized and Low-Overhead Implementations of Additive Schwarz Methods for High-Order FEM Multigrid Computations”. In: *The International Journal of High Performance Computing Applications* 38.3 (May 1, 2024), pp. 192–209. ISSN: 1094-3420. DOI: [10.1177/10943420231217221](https://doi.org/10.1177/10943420231217221).
- [50] P. Munch et al. “Efficient Distributed Matrix-free Multigrid Methods on Locally Refined Meshes for FEM Computations”. In: *ACM Transactions on Parallel Computing* 10.1 (Mar. 29, 2023), 3:1–3:38. ISSN: 2329-4949. DOI: [10.1145/3580314](https://doi.org/10.1145/3580314).
- [51] P. Munch et al. “Stage-Parallel Fully Implicit Runge–Kutta Implementations with Optimal Multilevel Preconditioners at the Scaling Limit”. In: *SIAM Journal on Scientific Computing* (July 18, 2023), S71–S96. ISSN: 1064-8275. DOI: [10.1137/22M1503270](https://doi.org/10.1137/22M1503270).
- [52] R. H. Nochetto, S. A. Sauter, and C. Wieners. “Space-Time Methods for Time-dependent Partial Differential Equations”. In: *Oberwolfach Reports* 14.1 (Jan. 2, 2018), pp. 863–947. ISSN: 1660-8933. DOI: [10.4171/owr/2017/15](https://doi.org/10.4171/owr/2017/15).
- [53] B. W. Ong and J. B. Schroder. “Applications of Time Parallelization”. In: *Computing and Visualization in Science* 23.1 (Sept. 23, 2020), p. 11. ISSN: 1433-0369. DOI: [10.1007/s00791-020-00331-4](https://doi.org/10.1007/s00791-020-00331-4).
- [54] L. F. Pavarino. “Additive Schwarz Methods for Thep-Version Finite Element Method”. In: *Numerische Mathematik* 66.1 (1 Dec. 1, 1993), pp. 493–515. ISSN: 0945-3245. DOI: [10.1007/BF01385709](https://doi.org/10.1007/BF01385709).
- [55] W. Pazner and P.-O. Persson. “Stage-Parallel Fully Implicit Runge–Kutta Solvers for Discontinuous Galerkin Fluid Simulations”. In: *Journal of Computational Physics* 335 (Apr. 15, 2017), pp. 700–717. ISSN: 0021-9991. DOI: [10.1016/j.jcp.2017.01.050](https://doi.org/10.1016/j.jcp.2017.01.050).
- [56] I. Perugia et al. “Tent Pitching and Trefftz-DG Method for the Acoustic Wave Equation”. In: *Computers & Mathematics with Applications* 79.10 (May 15, 2020), pp. 2987–3000. ISSN: 0898-1221. DOI: [10.1016/j.camwa.2020.01.006](https://doi.org/10.1016/j.camwa.2020.01.006).
- [57] J. Roth et al. “Tensor-Product Space-Time Goal-Oriented Error Control and Adaptivity With Partition-of-Unity Dual-Weighted Residuals for Nonstationary Flow Problems”. In: *Computational Methods in Applied Mathematics* (May 31, 2023). ISSN: 1609-9389. DOI: [10.1515/cmam-2022-0200](https://doi.org/10.1515/cmam-2022-0200).
- [58] F. Schieweck. “A-Stable Discontinuous Galerkin–Petrov Time Discretization of Higher Order”. In: *Journal of Numerical Mathematics* 18.1 (Jan. 2010). ISSN: 1570-2820, 1569-3953. DOI: [10.1515/jnum.2010.002](https://doi.org/10.1515/jnum.2010.002).
- [59] M. Schmich and B. Vexler. “Adaptivity with Dynamic Meshes for Space-Time Finite Element Discretizations of Parabolic Equations”. In: *SIAM J. Sci. Compu.* 30.1 (2008), pp. 369–393. DOI: [10.1137/060670468](https://doi.org/10.1137/060670468).
- [60] J. Schöberl et al. “Additive Schwarz Preconditioning for P-Version Triangular and Tetrahedral Finite Elements”. In: *IMA Journal of Numerical Analysis* 28.1 (Jan. 1, 2008), pp. 1–24. ISSN: 0272-4979. DOI: [10.1093/imanum/drl046](https://doi.org/10.1093/imanum/drl046).
- [61] O. Steinbach. “Space-Time Finite Element Methods for Parabolic Problems”. In: *Computational Methods in Applied Mathematics* 15.4 (Oct. 1, 2015), pp. 551–566. ISSN: 1609-9389. DOI: [10.1515/cmam-2015-0026](https://doi.org/10.1515/cmam-2015-0026).
- [62] O. Steinbach and H. Yang. “An Algebraic Multigrid Method for an Adaptive Space–Time Finite Element Discretization”. In: *Large-Scale Scientific Computing*. Ed. by I. Lirkov and S. Margenov. Lecture Notes in Computer Science. Cham: Springer International Publishing, 2018, pp. 66–73. ISBN: 978-3-319-73441-5. DOI: [10.1007/978-3-319-73441-5\\_6](https://doi.org/10.1007/978-3-319-73441-5_6).



- [63] O. Steinbach and M. Zank. “Coercive Space-Time Finite Element Methods for Initial Boundary Value Problems”. In: *ETNA - Electronic Transactions on Numerical Analysis* 52 (2020), pp. 154–194. ISSN: 1068-9613, 1068-9613. DOI: [10.1553/etna\\_vol52s154](https://doi.org/10.1553/etna_vol52s154).
- [64] Y. Sun, S.-L. Wu, and Y. Xu. “A Parallel-in-Time Implementation of the Numerov Method For Wave Equations”. In: *Journal of Scientific Computing* 90.1 (1 Jan. 1, 2022), pp. 1–31. ISSN: 1573-7691. DOI: [10.1007/s10915-021-01701-x](https://doi.org/10.1007/s10915-021-01701-x).
- [65] R. Tielen, M. Möller, and C. Vuik. “Combining P-Multigrid and Multigrid Reduction in Time Methods to Obtain a Scalable Solver for Isogeometric Analysis”. In: *SN Applied Sciences* 4.6 (May 10, 2022), p. 163. ISSN: 2523-3971. DOI: [10.1007/s42452-022-05043-7](https://doi.org/10.1007/s42452-022-05043-7).
- [66] U. Trottenberg, C. W. Oosterlee, and A. Schuller. *Multigrid*. Elsevier, Nov. 20, 2000. 648 pp. ISBN: 978-0-08-047956-9.
- [67] P. S. Vassilevski. *Multilevel Block Factorization Preconditioners: Matrix-based Analysis and Algorithms for Solving Finite Element Equations*. Springer, Oct. 22, 2008. 527 pp. ISBN: 978-0-387-71564-3.
- [68] H. Wobker and S. Turek. “Numerical Studies of Vanka-Type Smoothers in Computational Solid Mechanics”. In: *Adv. Appl. Math. Mech.* (2009).